

000 BEYOND MARKOV ASSUMPTION: IMPROVING SAMPLE 001 EFFICIENCY IN MDPs BY HISTORICAL AUGMENTATION 002

003 **Anonymous authors**

004 Paper under double-blind review

005 ABSTRACT

006 Under the Markov assumption of Markov Decision Processes (MDPs), an optimal
007 stationary policy does not need to consider history and is no worse than any non-
008 stationary or history-dependent policy. Therefore, existing Deep Reinforcement
009 Learning (DRL) algorithms usually model sequential decision-making as an MDP
010 and then try to optimize a stationary policy by single-step state transitions. How-
011 ever, such optimization is often faced with sample inefficiency when the causal
012 relationships of state transitions are complex. To address the above problem, this
013 paper investigates if augmenting the states with their historical information can
014 simplify the complex causal relationships in MDPs and thus improve the sample
015 efficiency for DRL. First, we demonstrate that a complex causal relationship of
016 single-step state transitions may be inferred by a simple causal function of the
017 historically augmented states. Then, we propose a convolutional neural network
018 architecture to learn the representation of the current state and its historical tra-
019 jectory. This representation learning compresses the high-dimensional historical
020 trajectories into a low-dimensional space to extract the simple causal relationships
021 from historical information and avoid the overfitting caused by high-dimensional
022 data. Finally, we formulate Historical Augmentation Aided Actor-Critic (HA3C)
023 algorithm by adding the learned representations to the actor-critic method. The
024 experiment on standard MDP tasks demonstrates that HA3C outperforms current
025 state-of-the-art methods in terms of both sample efficiency and performance.

030 1 INTRODUCTION

031 Sequential decision-making widely exists in real-world control tasks, such as robot control and
032 autonomous driving (Dorf & Bishop, 2011; Ibarz et al., 2021; Sallab et al., 2017). Generally speaking,
033 it can be modelled as a Markov Decision Process (MDP), where an agent iteratively takes action in an
034 environment for transiting from one state to another (Puterman, 1990). Each transition is evaluated by
035 a reward signal passing from the environment to the agent so that Reinforcement Learning (RL) can
036 learn the optimal policy by maximizing the cumulative reward (Sutton & Barto, 2018). The Markov
037 assumption of MDPs asserts that the probability distributions of the reward and next state depend
038 only on the current state and action. Under the Markov assumption of MDPs, there exists an optimal
039 stationary policy which does not need to consider history and is no worse than any non-stationary or
040 history-dependent policy (Puterman, 2014). Therefore, existing RL algorithms usually try to optimize
041 a stationary policy by single-step state transitions.

042 With advances in deep learning, many effective Deep RL (DRL) methods were proposed (Fujimoto
043 et al., 2018; Haarnoja et al., 2018; Lillicrap et al., 2016; Mnih et al., 2016; 2015). Under the Markov
044 assumption of MDPs, they are usually based on the actor-critic method where the critic estimates
045 the Q -function, i.e., the expected cumulative reward after taking action at each state, while the actor
046 updates the policy to choose the action which can maximize the estimated Q -function (Schulman
047 et al., 2015; Silver et al., 2014). However, such optimization may miss the useful causal relationships
048 of state transitions, leading to sample inefficiency (Allen et al., 2021; Buckman et al., 2018; Du
049 et al., 2020; Guo et al., 2020). An existing partial solution to this issue is representation learning in
050 which a neural network is trained to infer the causal relationships of state transitions by predicting the
051 reward or future state of each state-action pair (Munk et al., 2016; Ni et al., 2023; Ravindran, 2004;
052 Rezaei-Shoshtari et al., 2022). Then, the sample efficiency of DRL can be improved by adding the
053 learned representations to the actor-critic method. Unfortunately, it is hard to train the neural networks

054 which can infer complex causal relationships, e.g., polynomial causal relationships and the basic laws
 055 of physics (Andoni et al., 2014; Cranmer et al., 2020). Standard complexity-theoretic results strongly
 056 suggest that there is no algorithm efficient enough for learning arbitrary target functions, even for
 057 target functions representable by very low-depth networks (Applebaum et al., 2006). Therefore, the
 058 sample efficiency for DRL is still limited in complex MDP tasks.

059 This paper addresses the above problem by augmenting the states with their historical information.
 060 Based on the analysis and example in Section 3, we believe that **although satisfying Markov**
 061 **assumption, an MDP may have its inherent contextual information.** In this case historical
 062 augmentation can simplify the causal relationships of state transitions of this MDP by increasing the
 063 search space of the causal functions (Hallak et al., 2015; Sprunger & Jacobs, 2019). Therefore, we
 064 focus on optimizing a history-dependent stationary policy in an MDP. Our DRL approach comprises
 065 two key components: 1) Learning the state representations to capture the causal relationships in an
 066 MDP and 2) finding the optimal stationary policy by the learned representations. Given an action and
 067 the historically augmented current state, our representation learning utilizes a Convolutional Neural
 068 Network (CNN) architecture to compress the high-dimensional historical trajectory of the given state
 069 into a low-dimensional space while predicting the future state. The compressed historical trajectories
 070 can be seen as the abstracted features which can represent the simple causal relationships and avoid
 071 the overfitting caused by high-dimensional data (Andre & Russell, 2002). To keep the Markov
 072 assumption of MDPs, our representation learning does not compress the current state. We add the
 073 learned state representations to the actor-critic method. In this way, the causal relationships captured
 074 by our representation learning can be utilized to estimate the Q -function and update policy. Therefore,
 075 our new DRL approach can optimize the policy in a complex MDP with high sample efficiency. We
 076 combine historical augmentation, state representations, and TD3 in our approach to formulate a new
 077 DRL algorithm, Historical Augmentation Aided Actor-Critic (HA3C). The experiment on standard
 078 MDP tasks, i.e. Mujoco control tasks and Deep Mind Control (DMC) suite, empirically demonstrates
 079 that HA3C outperforms current state-of-the-art methods in terms of both sample efficiency and
 080 performance (Brockman et al., 2016; Todorov et al., 2012; Tassa et al., 2018).

081 Our contributions are as follows: 1) It is the first time in the literature that historical augmentation
 082 can be used to improve sample efficiency when Markov assumption is satisfied. 2) We propose a
 083 new DRL approach to address the problem of how to effectively utilize the historical information in
 084 MDPs. 3) Based on this approach, we formulate a new RL algorithm, HA3C, which outperforms
 085 existing state-of-the-art DRL algorithms, e.g. TD7 (Fujimoto et al., 2023).

086 2 BACKGROUND

087 An MDP can be written as a 5-tuple $\mathbb{M} = \langle \mathcal{S}, \mathcal{A}, R, \mathbf{P}, \gamma \rangle$ with state space \mathcal{S} , action space \mathcal{A} , reward
 088 function R , transition model \mathbf{P} , and discount factor γ . In an MDP, RL can maximize the discounted
 089 cumulative reward by learning how to map the states to the actions (Baird, 1995; Duan et al., 2016;
 090 Williams, 1992). For a given state $s_t \in \mathcal{S}$ at time step t , the agent executes an action $a_t \in \mathcal{A}$ w.r.t. a
 091 policy $\pi : \mathcal{S} \mapsto \mathcal{A}$, to obtain a reward $r_t = R(s_t, a_t)$ and transfer to a new state s_{t+1} . The return of
 092 the agent is defined as the discounted cumulative reward $G_t = \sum_{i=t}^{+\infty} \gamma^{i-t} r_i$. Based on the Markov
 093 assumption of MDPs, RL can find the optimal policy to maximize the following value function which
 094 is the expected return when $s_t = s$ and following π thereafter.
 095

$$096 \quad V^\pi(s) = \mathbb{E}^\pi [G_t | s_t = s] = \mathbb{E}^\pi \left[\sum_{i=0}^{+\infty} \gamma^i r_{t+i} | s_t = s \right],$$

097 where $\mathbb{E}^\pi [\cdot]$ denotes the expected value of a random variable given that the agent follows policy π .

100 With advances in deep learning, combining neural networks into RL has drawn significant attention
 101 in the literature. Many DRL algorithms learn the optimal policy by the actor-critic method (Kaelbling
 102 et al., 1996), where the critic network estimates the Q -function which is the expected return when
 103 $s_t = s, a_t = a$, and following policy π thereafter.

$$104 \quad Q^\pi(s, a) = \mathbb{E}^\pi [G_t | s_t = s, a_t = a] = \mathbb{E}^\pi \left[\sum_{i=0}^{+\infty} \gamma^i r_{t+i} | s_t = s, a_t = a \right],$$

105 while the actor network updates the policy to maximize the estimated Q -function.

108 To improve sample efficiency, some DRL methods learn the state representations of the collected
 109 state transitions and then add the learned representations to the actor-critic method (Anand et al.,
 110 2019; Dayan, 1993; Gelada et al., 2019; Li et al., 2006). This representation learning aims to
 111 capture the causal relationships in MDPs, and thus improves sample efficiency (Liu et al., 2020;
 112 Van Hoof et al., 2016; Ye et al., 2023; Zhang et al., 2021). For example, ML-DDPG learns the state
 113 representations by predicting the next state representation and the reward in MDPs (Munk et al.,
 114 2016). As an improvement of ML-DDPG, OFENet learns the high-dimensional state representations
 115 by predicting the next state in DenseNet architecture (Ota et al., 2020). TD7 improves the learning
 116 of state representations by AvgL1Norm and then combines the learned representations with TD3,
 117 checkpoints, and prioritized replay buffer (Fujimoto et al., 2023).

118 DRL algorithms need to consider historical information when the Markov assumption of MDPs
 119 is violated (Eysenbach et al., 2020; Majeed & Hutter, 2018; Hafner et al., 2019b). For Partially
 120 Observable MDPs (POMDPs), in which the states are partially observable, deep recurrent Q -network
 121 uses LSTMs to encode state transition trajectories in the Q -function estimation (Hausknecht &
 122 Stone, 2015). As an improvement of deep recurrent Q -network, deep transformer Q -network uses
 123 transformers to encode the state transition trajectories (Esslinger et al., 2022). As a famous DRL
 124 algorithm, Dreamer encodes the historical information into the state at every time step in POMDPs (Ha
 125 & Schmidhuber, 2018; Hafner et al., 2019a). In delayed MDPs, in which the current state and reward
 126 may arrive at the agent with a delay (Katsikopoulos & Engelbrecht, 2003), researchers usually recover
 127 the Markov assumption of MDPs by considering the historical actions (Bouteiller et al., 2020; Derman
 128 et al., 2021). When the Markov assumption of MDPs is violated by the state abstraction, it is possible
 129 to find a history-based policy which works in the abstracted space and is of the same quality as
 130 optimal policy (Patil et al., 2024). However, the history-based DRL for the dynamics which are under
 131 Markov assumption is largely absent from the literature.

132 3 MOTIVATION

133 Let $\mathbf{h}_t = \{s_0, a_0, \dots, s_t\}$ as the history up to time step t in a sequential decision-making task. The
 134 optimal policy may change the decision rule in different time steps and select actions based on
 135 historical information. In this case, we should optimize a history-dependent policy $\pi = \{d_t | t = 0, 1, \dots\}$ which
 136 selects action at time step t by decision-rule $d_t(a_t | \mathbf{h}_t)$. Fortunately, based on the
 137 Markov assumption of MDPs, there is an optimal stationary policy $\pi(a_t | s_t)$ which is unrelated to
 138 time and selects action a_t by only the state s_t . This Markov assumption asserts that the probability
 139 distributions of state s_{t+1} and reward r_t depend only on the s_t and a_t as

$$141 P\{s_{t+1} = s', r_t = r | s_0, a_0, r_0, \dots, s_t, a_t\} = P\{s_{t+1} = s', r_t = r | s_t, a_t\},$$

142 where P is the probability distribution in \mathbf{P} . Let HR and SR denote the class of history-dependent
 143 and stationary policies, respectively. Lemma 3.1 is the key of most existing RL algorithms (Puterman,
 144 2014)[Thm. 6.2.10]. The different types of policies are detailed in Appendix A.

145 **Lemma 3.1.** *Under the Markov assumption of MDPs, there exists a policy $\pi^* \in SR$ such that, for
 146 all t , $V_{\pi^*}(s_t) = \sup_{\pi \in HR} V_{\pi}(\mathbf{h}_t)$.*

147 Based on Lemma 3.1, existing DRL algorithms for MDPs usually optimize a stationary policy by
 148 single-step transitions. If the causal relationships in the modelled MDP are simple, e.g., there are
 149 only linear causal relationships in this MDP, such optimization effectively finds the optimal policy.
 150 A classical result is that a neural network with a single hidden layer can successfully learn a linear
 151 function (Andoni et al., 2014). However, it is still hard to capture complex causal relationships by
 152 neural networks. Standard complexity-theoretic results strongly suggest that there is no algorithm
 153 efficient enough for learning arbitrary functions, even for target functions representable by very
 154 low-depth networks (Applebaum et al., 2006). In fact, a more complex causal function requires
 155 neural networks to approximate with more parameters, samples, and time consumption (Bianchini &
 156 Scarselli, 2014).

157 **Although satisfying Markov assumption, many MDPs in real-world applications have their
 158 historical contextual information.** In this case, historical augmentation can address the above
 159 problem by simplifying the causal relationships in these MDPs as it can increase the search space
 160 of the causal functions to mine the contextual information on state transitions (Hallak et al., 2015;
 161 Sodhani et al., 2022). For example, if we model the state transitions with Fibonacci sequence as

162 $s_0 = 1, s_1 = 1, s_2 = 2, s_3 = 3, s_4 = 5, \dots$, when $t > 2$, the state transitions in this model will
 163 satisfy the Markov assumption of Markov Processes as (Dynkin, 1965)

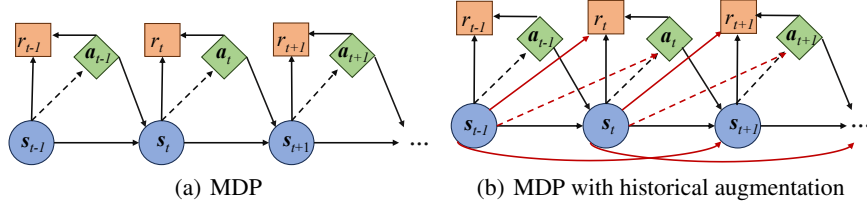
$$165 P\{s_{t+1} = s' | s_0, \dots, s_t\} = P\{s_{t+1} = s' | s_t\}.$$

166 Without considering history, at s_t , it is hard to predict s_{t+1} . Fortunately, when considering history,
 167 we can predict s_{t+1} by a simple linear function

$$169 s_{t+1} = s_{t-1} + s_t.$$

170 A toy experiment on Fibonacci sequence is shown in Appendix B.

172 In Appendix C, we give two other examples to illustrate that by historical augmentation, a com-
 173 plex causal relationship in single-step transitions may be simplified as a linear causal relationship.
 174 Fig. 1(a) presents the original MDP causal relationships and Fig. 1(b) demonstrates the MDP causal
 175 relationships with state augmentation. When inferring the causal relationships in a trajectory, the



184 Figure 1: Causal diagrams of an MDP with or without historical augmentation. The black lines index
 185 the original MDP causal relationships and the red lines index the causal relationships from historical
 186 augmentation. The dashed lines indicate the information needed in the optimization.

187 causal function in Fig 1(b) can be simpler than the causal function in Fig 1(a).

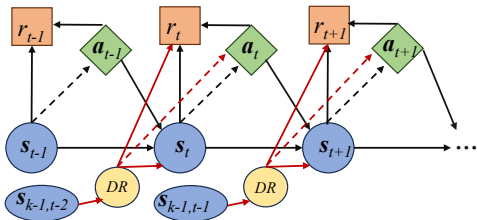
190 From the analysis above, the motivation of our work is that historical information can simplify the
 191 complex causal relationships in MDPs and thus has the potential to improve the sample efficiency
 192 of DRL. However, the challenges are 1) how to ensure that the causal relationships learned from
 193 historical augmentation are simple and 2) avoiding overfitting caused by the high-dimensional
 194 historical data.

195 4 METHOD

198 In this section, we propose a new DRL approach
 199 by the representation learning of historically
 200 augmented states. Then, we formulate a new
 201 DRL algorithm, HA3C, and illustrate the advan-
 202 tage of this algorithm with a visual example.

203 4.1 REPRESENTATION LEARNING 204 ON HISTORICALLY AUGMENTED STATES

206 To address the problem of how to effectively
 207 utilize the historical information in MDPs, we
 208 propose a new DRL approach by the represen-
 209 tation learning of historically augmented states.
 210 The main idea of this representation learning
 211 is to compress the high-dimensional historical
 212 trajectories into a low-dimensional represen-
 213 tation space (Andre & Russell, 2002; Li et al., 2006). On the one hand, the compressed historical
 214 trajectories can be seen as the abstracted features of the historical information to extract the simple
 215 causal relationships. On the other hand, this compression will avoid the overfitting caused by the
 high-dimensional historical data (Ying, 2019).



802 Figure 2: Causal diagram of a historically aug-
 803 mented MDP with state abstraction. DR represents
 804 the operation of dimensionality reduction.

To keep the Markov assumption of MDPs, our representation learning does not compress the current state. Let $s_{k,t} = \{s_{t-k+1}, \dots, s_t\}$. If $t < k$, one can set each $s_i \in s_{k-t-1}$ by the zero vector $\mathbf{0}$. The causal diagram of MDP with our state abstraction is in Fig. 2. As we can see, when predicting s_{t+1} by $s_{k,t}$ and a_t , the dimensionality reduction is only performed on $s_{k-1,t-1}$. **A theoretical analysis of sample complexity reduction from historical augmentation is shown in Appendix E.**

Let $S_k D$ denote the class of the stationary deterministic policies based on k -order state trajectories. Theorem 4.1 forms the basis of our DRL approach. This theorem can be implied by Lemma 3.1. For completeness, we provide a proof in Appendix E.

Theorem 4.1. *Under the Markov assumption of MDPs, there exists a stationary deterministic policy $\mu^* \in S_k D$ such that, for all t , $V^{\mu^*}(s_{k,t}) = \sup_{\pi \in HR} V^\pi(h_t)$.*

To capture the simplified causal relationships in MDPs by historical augmentation, we define a pair of encoders $\mathbf{z}^{s_{k,t}} = f(s_{k,t})$ and $\mathbf{z}^{s_{k,t}, a_t} = g(\mathbf{z}^{s_{k,t}}, a_t)$. Based on the Markov assumption in MDPs, we can predict $\mathbf{z}^{s_{k,t+1}}$, i.e., the representation of $s_{k,t+1}$, by $\mathbf{z}^{s_{k,t}, a_t}$. Thus, the two encoders are trained by minimizing the following predicting loss:

$$L(f, g) = \|g(f(s_{k,t}), a_t) - f(s_{k,t+1})\|_2^2 = \|\mathbf{z}^{s_{k,t}, a_t} - \mathbf{z}^{s_{k,t+1}}\|_2^2, \quad (1)$$

where $|\cdot|_x$ denotes the stop-gradient operation. As presented in Fig. 3, a simple yet effective CNN network architecture is utilized in our representation learning. In the network of $f(s_{k,t})$, we first use a CNN layer to mine the historical information in $s_{k-1,t-1}$. This layer produces the feature maps of $s_{k-1,t-1}$ by the multiple filters, which are as wide as the state dimensionality. Second, we utilize a max pooling layer to capture the most important features and an average pooling layer to capture the tendency features. Third, we compress the captured features into a low-dimensional space and learn the features of s_t . Finally, we concatenate the compressed features of $s_{k-1,t-1}$ and the learned features of s_t . The concatenated features are the input of the next fully connected layer to obtain the representation $\mathbf{z}^{s_{k,t}}$. In the network of $g(\mathbf{z}^{s_{k,t}}, a_t)$, we put the concatenation of $\mathbf{z}^{s_{k,t}}$ and a_t into the two fully connected layers to obtain the representation $\mathbf{z}^{s_{k,t}, a_t}$.

We combine our learned representations with the actor-critic method and thus the Q -function can be defined as $\hat{Q}(\mathbf{z}^{s_{k,t}}, a_t)$ and the policy can be defined as $\mu(\mathbf{z}^{s_{k,t}}) \in S_k D$. Define the probability distribution of $\mathbf{z}^{s_{k,t+1}}$ under μ as

$$P^\mu\{\mathbf{z}^{s_{k,t+1}} = \mathbf{z}^{s'_{k,:}} | \mathbf{z}^{s_{k,:}} = \mathbf{z}^{s_{k,:}}\} = \int_{\mathcal{Z}} \mathbb{E}_{a \sim \mu(\mathbf{z}^{s_{k,:}})} [p(\mathbf{z}^{s'_{k,:}} | \mathbf{z}^{s_{k,:}}, a)] d\mathbf{z}^{s_{k,:}},$$

where $s_{k,:}$ is a k -order state trajectory $\{s_0, \dots, s_{k-1}\}$ ending with s , i.e., $s_{k-1} = s$, \mathcal{Z} is the set of all possible $\mathbf{z}^{s_{k,:}}$, and $p(\mathbf{z}^{s'_{k,:}} | \mathbf{z}^{s_{k,:}}, a)$ is the probability of transferring to $\mathbf{z}^{s'_{k,:}}$ with taking a at $\mathbf{z}^{s_{k,:}}$. Our optimization is based on a Bellman optimality operator B for μ as

$$B_\mu \hat{Q}(\mathbf{z}^{s_{k,:}}, a) = \max_{\mu} \mathbb{E}_{a_{t+1} \sim \mu, \mathbf{z}^{s_{k,t+1}} \sim P^\mu} [r_t + \gamma \hat{Q}(\mathbf{z}^{s_{k,t+1}}, a_{t+1})]. \quad (2)$$

The following theorem gives the conditions to find the optimal stationary policy in our approach. The proof of this theorem is given in Appendix E.

Theorem 4.2. *Given a finite MDP, if 1) $f(*)$ and $g(*)$ are fixed, 2) $\forall s_{k,:}, s'_{k,:} \in \mathcal{S}_{k,:}, s \neq s' \Leftrightarrow \mathbf{z}^{s_{k,:}} \neq \mathbf{z}^{s'_{k,:}}$, and 3) $L(f, g) \rightarrow 0$, then $\hat{Q}(\mathbf{z}^{s_{k,t}}, a_t)$ converges to the optimal $Q^*(s_t, a_t)$ by the Bellman optimality operator in equation 2.*

This theorem illustrates that no matter whether different historical trajectories lead to different representations on the state s , we can still find the optimal stationary policy in the representation space. To make condition 2) hold, we can increase the dimensionality of s in representation learning. This operation also can improve sample efficiency (Ota et al., 2020). To see condition 3) hold, there should exist a $s'_{k,:}$ that satisfies

$$p\{s_{k,t+1} = s'_{k,:} | s_{k,t}, a_t\} \rightarrow 1.$$

270

271

272 There is an analysis of the function approxima-
 273 tion error in Appendix E. We add $z^{s_{k,t}, a_t}$ to \hat{Q}
 274 to consider the learned relationship between a_t
 275 and $z^{s_{k,t}}$ in the representation space. We also
 276 add s_t to \hat{Q} and μ to consolidate the rela-
 277 tionships in single-step transitions. Thus Q and μ
 278 can be written as $\hat{Q}(z^{s_{k,t}, a_t}, z^{s_{k,t}}, s_t, a_t)$ and
 279 $\mu(z^{s_{k,t}}, s_t)$, respectively. The operations in \hat{Q}
 280 and μ are shown in Fig. 4. Our approach can
 281 be connected with POMDPs, High-order MDPs
 282 (HMDPs), and state abstraction. A detailed analysis of the connections between our approach and the
 283 related work is shown in Appendix D.

284

285

4.2 HA3C ALGORITHM

286

287 In this subsection, we propose HA3C algorithm which is a combination of TD3, representation
 288 learning, historical augmentation. HA3C has several networks as follows. Two critic networks
 289 ($\hat{Q}_{\phi_1}, \hat{Q}_{\phi_2}$), two target critic networks ($\hat{Q}_{\phi_1^T}, \hat{Q}_{\phi_2^T}$), an actor network μ_θ , a target actor network μ_{θ^T} ,
 290 two encoders (f_σ, g_σ), two fixed encoders ($f_{\sigma^F}, g_{\sigma^F}$), two target encoders ($f_{\sigma^T}, g_{\sigma^T}$), a checkpoint
 291 actor network π_{θ^C} , and a checkpoint encoder f_{σ^C} .

292

293 To learn the representations with historical augmentation, f_σ , and g_σ are trained by the transitions in
 294 buffer $\mathcal{B} = \{s_{k,i}, a_i, r_i, s_{k,i+1}\}$ to minimize the predicting loss in equation 1. For any parameter set
 α , we define

295

$$z_\alpha^{s_{k,t}} = f_\alpha(s_{k,t}), \quad z_\alpha^{s_{k,t}, a_t} = g_\alpha(z^{s_{k,t}}, a_t).$$

296

297 Based on the assumption that f_{σ^F} and g_{σ^F} satisfy the conditions in Theorem 4.2 on the most
 298 transitions in \mathcal{B} , the \hat{Q} -function is estimated by the following Huber loss function (Huber, 1992).

299

$$L(\phi_i) = H_{(s_{k,:}, a, r) \sim \mathcal{B}} [x_t - (\hat{Q}_{\phi_i}(z_{\sigma^F}^{s_{k,t}, a_t}, z_{\sigma^F}^{s_t}, s_t, a_t)], \quad (3)$$

300

$$x_t = r_t + \gamma \text{clip}(\min(\hat{Q}_{\phi_i^T}(z_{\sigma^T}^{s_{k,t+1}, a'}, z_{\sigma^T}^{s_{t+1}}, s_{t+1}, a')), \hat{Q}^{\min}, \hat{Q}^{\max}),$$

301

$$a' = \mu_{\theta^T}(z_{\sigma^T}^{s_{k,t+1}}, s_{t+1}) + \epsilon_T, \epsilon_T \sim \mathcal{N},$$

302

303 where ϵ_T is target policy noise (Fujimoto et al., 2018), \mathcal{N} is a Gaussian distribution $\mathcal{N}(0, \sigma)$, and
 304 \hat{Q}^{\min} and \hat{Q}^{\max} are updated at each time step as

305

$$\hat{Q}^{\max} \leftarrow \max(x_t, \hat{Q}^{\max}), \quad \hat{Q}^{\min} \leftarrow \min(x_t, \hat{Q}^{\min}).$$

306

307 Based on the learned Q -function, the policy network π_θ is updated by

308

$$\max_\theta \mathbb{E}_{s_{k,t} \sim \mathcal{B}} \left[\sum_{i=1,2} \hat{Q}_{\phi_i}(z^{s_{k,t}, a}, z^{s_t}, s_t, a) \right], \quad (4)$$

309

$$a = \mu_\theta(z_{\sigma^F}^{s_{k,t}}, s_t).$$

310

311

312 To explore the new actions and thus generate new transitions in \mathcal{B} , exploration noise ϵ is added as

313

$$a_t \leftarrow a_t + \epsilon_e, \epsilon_e \sim \mathcal{N}.$$

314

315 In our TD learning, σ^F , σ^T , ϕ^T , and θ^T are updated by

316

$$\sigma^F \leftarrow \sigma^T, \quad \sigma^T \leftarrow \sigma, \quad \phi^T \leftarrow \phi, \quad \theta^T \leftarrow \theta. \quad (5)$$

317

318 Because DRL algorithms are unstable (Henderson et al., 2018; Teh et al., 2017), we use the checkpoint
 319 policy to obtain the cumulative reward in our evaluation (Vaswani et al., 2017). In the training of
 320 HA3C, if the current policy outperforms the checkpoint policy, we will update the checkpoint policy
 321 with the current policy, then $\sigma^C \leftarrow \sigma$ and $\theta^C \leftarrow \theta$. The checkpoint policy can give a more accurate
 322 evaluation by maintaining the high-performance policy unchanged. Furthermore, the LAP replay
 323 buffer is utilized to store and replay the transitions (Fujimoto et al., 2023; 2020). The pseudo code of
 324 online HA3C is presented in Appendix F.

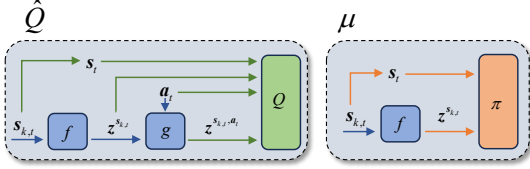


Figure 4: The operations in Q and μ .

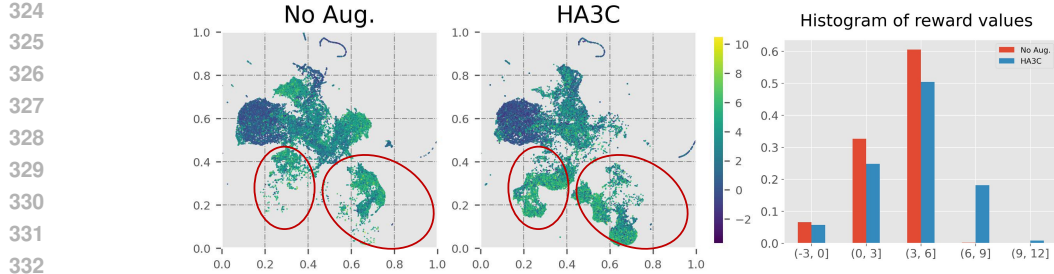


Figure 5: Visual results of the obtained states in Walker2d environment. Each state is coloured by the reward of reaching this state. The red circles index the high-reward states, which can be more frequently reached by the historical augmentation policy.

Fig. 5 is an example to illustrate the advantage of learning the policy in HA3C. We first collect the obtained states of Walker2d MuJoCo control task by learning the policy with and without historical augmentation, respectively. The max learning step is 4×10^5 . Then we map the collected states in 2D space together by UMAP. Finally, we show the reached states without the learning of historical augmentation in the left subfigure of Fig. 5 and the reached states with the learning of historical augmentation in the middle subfigure of Fig. 5. Each state is coloured by the reward of reaching it. As we can see, although the actions to obtain the states in high-reward regions (indexed by the red circles) can be explored, without historical augmentation, it is hard to learn the policy which can regenerate these explored actions. Therefore, in the left subfigure, there are only a few states in the high-reward regions. Fortunately, as shown in the middle subfigure, there are a lot of states in the high-reward regions when learning the policy with historical augmentation. The histogram of the rewards in the right subfigure of Fig. 5 also demonstrates the advantage of HA3C.

5 EXPERIMENTAL RESULT

In this section, first, we compare HA3C to five existing RL algorithms on five Mujoco control tasks (Todorov et al., 2012). Then, we give the ablation study of HA3C to illustrate that historical augmentation is the real source of the improvement in sample efficiency. Finally, we analyze the parameter sensitivity on the length of the historical state trajectory and the number of dimensions of compressed historical trajectories. The experimental setting is in Appendix G. Appendix H has some supplementary experiments, including **BipedWalker experiment**, **DMC experiment**, **HA3C-SAC experiment**, **HA3C-LSTM experiment**, **the comparison between HA3C and CrossQ (Bhatt et al., 2024)**, **running time analysis**, and **the state visualization**.

5.1 COMPARATIVE EVALUATION

In this subsection, we evaluate our HA3C on five MuJoCo control tasks including Walker2d, HalfCheetah, Ant, Humanoid, and Hopper. The compared algorithms are TD3 (Fujimoto et al., 2018), SAC (Haarnoja et al., 2018), TQC (Kuznetsov et al., 2020), TD3+OFE (Ota et al., 2020), and TD7 (Fujimoto et al., 2023). For all algorithms, each task runs 10 instances with different random seeds. In each instance, the evaluation is performed every 5000 time steps. The learning curves are shown in Fig. 6 and the numerical results at 300K time step and 3M time step are shown in Table 1.

From Fig. 6 and Table 1, we can see that 1) with the help of historical augmentation, HA3C significantly outperforms the compared algorithms in terms of the early average highest returns (300K time step) and final average highest returns (3M time step); 2) TD3+OFE improves TD3 by the state representation, therefore, the results of TD3+OFE are better than the results of TD3. 3) With the help of AvgL1Norm, checkpoints, and prioritized replay buffer, TD7 get the better results than TD3+OFE.

5.2 ABLATION STUDY

Our ablation study aims to prove that our historical augmentation is the real source of the improvement in sample efficiency. Therefore, we compare HA3C to the following two ablations: 1) Copy Aug.

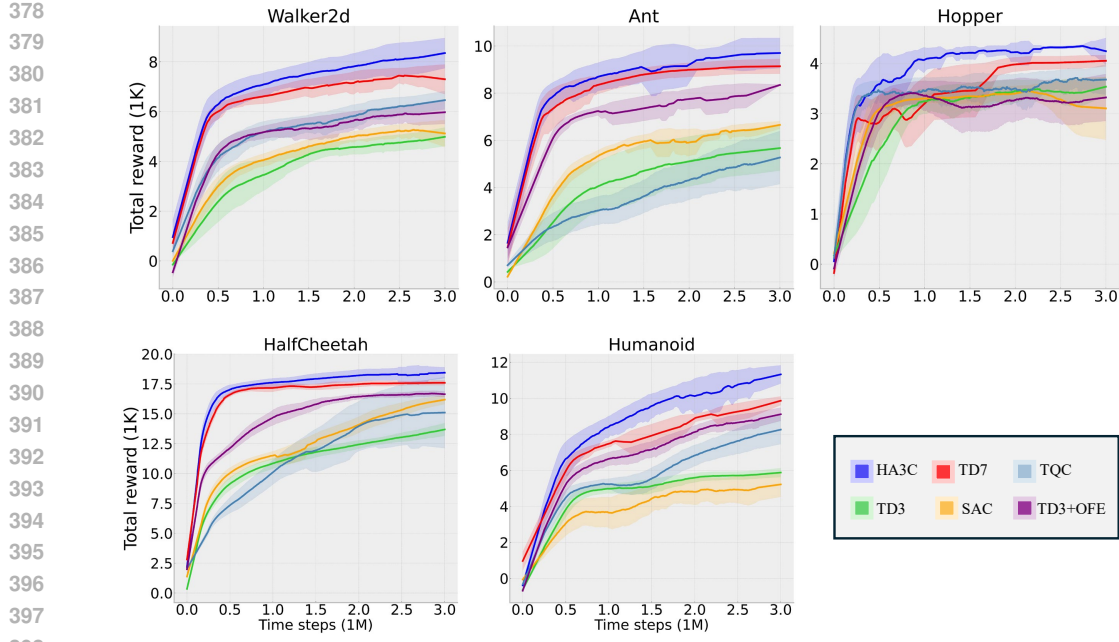


Figure 6: Learning curves of different RL algorithms on the MuJoCo control tasks. The shaded area captures a 90% confidence interval around the average performance.

Table 1: The average highest returns over 10 instances on the MuJoCo control tasks at 300K and 3M time steps. \pm captures the standard deviation over trials. The best score is highlighted by **cyan** and the second best score is highlighted by **orange**.

Algorithm	Time step	Walker2d	HalfCheetah	Ant	Humanoid	Hopper
TD3	300K	1848 \pm 947	7644 \pm 570	1540 \pm 1108	2202 \pm 807	2130 \pm 825
	3M	5150 \pm 428	14085 \pm 613	5819 \pm 1216	6159 \pm 202	3655 \pm 131
SAC	300K	2720 \pm 433	8770 \pm 679	2366 \pm 375	2507 \pm 535	3240 \pm 116
	3M	5575 \pm 149	16414 \pm 532	6892 \pm 269	5894 \pm 136	3637 \pm 124
TQC	300K	4210 \pm 235	6199 \pm 248	2778 \pm 407	3785 \pm 928	3594 \pm 47
	3M	6706 \pm 370	15742 \pm 974	7672 \pm 1171	8795 \pm 991	3972 \pm 77
TD3+OFE	300K	4016 \pm 219	11085 \pm 485	5897 \pm 483	4687 \pm 441	3251 \pm 204
	3M	6321 \pm 312	17187 \pm 165	8391 \pm 193	9632 \pm 273	3942 \pm 154
TD7	300K	5719 \pm 174	15002 \pm 240	7091 \pm 679	6043 \pm 159	3323 \pm 60
	3M	7670 \pm 321	17787 \pm 286	9225 \pm 450	9850 \pm 226	4049 \pm 156
HA3C	300K	6036 \pm 429	16415 \pm 437	7488 \pm 389	6248 \pm 118	3607 \pm 106
	3M	8563 \pm 829	18687 \pm 683	9794 \pm 891	11521 \pm 412	4413 \pm 59

copies the current state k times instead of augmenting with k steps of history in our CNN; 2) No Aug. is TD3 with single-step representation learning and LAP. Our ablation study is performed on Ant, Hopper, and Walker2d. All of the comparison methods have the same parameter setting.

As we can see from Fig. 7, HA3C significantly outperforms the compared algorithms in terms of both sample efficiency and performance on Ant and Walker2d. HA3C also significantly outperforms the compared algorithms in final performance on Hopper. This phenomenon illustrates that historical augmentation is the real source for improving sample efficiency.

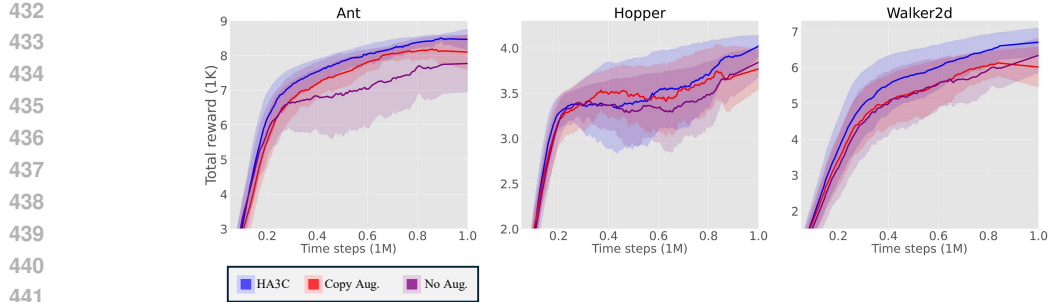


Figure 7: Learning curves of the ablation study on the MuJoCo benchmark.

5.3 PARAMETER SENSITIVITY ANALYSIS

In Fig. 8, we analyze the sensitivities of two important parameters, k and N , on Ant. k is the length of the historical state trajectory and N is the number of dimensions of compressed historical trajectories. Both of the above parameters are not used in the previous representation-based RL algorithms. k is set from $\{4, 6, 12, 18, 24\}$ and N is set from $\{6, 8, 16, 64, 256\}$.

As we can see, HA3C is a little sensitive to k and N . When $k \leq 12$ and $N \leq 16$, our historical augmentation will significantly improve the sample efficiency. When $N = 256$, the historical information cannot improve neither sample efficiency nor final performance. This phenomenon illustrates that compressing the historical trajectories into a low-dimensional space is the key to effectively utilize the historical information in MDP tasks. On the one hand, the low-dimensional representation may **simplify the complex causal relationships**. On the other hand, it will avoid the overfitting caused by the high-dimensional historical data (Ying, 2019). The performance is instability when $k = 24$. This may be because when the length of the considered historical trajectories exceeds the length required to extract latent contexts, noise will be generated in the representations.

6 CONCLUSION

Under the Markov assumption of MDPs, the probability distributions of the next state and reward depend only on the current state and action. Therefore, given a finite Q -table, we can find the optimal policy in an MDP by a heuristic algorithm which only considers single-step transitions. Different from the heuristic algorithm, DRL algorithms need to approximate the causal functions by learning the causal relationships in MDPs. In this case, DRL is often faced with sample inefficiency from complex causal relationships, as a more complex causal function requires neural networks to approximate with more parameters, samples, and time consumption.

Inspired by Hallak et al. (2015), to maximize the cumulative reward, the neural networks need to learn the underlying latent contexts in MDPs. When these contexts are hidden in the historical trajectories, historical information can be the "prompt" that simplifies the prediction of the next state. Therefore, we focus on optimizing a history-dependent stationary policy in MDPs and propose a new RL algorithm, HA3C. The value of k depends on how many transition steps can present the learnable context for DRL. If we expand the example of the Fibonacci sequence as $s_{t+1} = \sum_{i=t-m}^t s_i$, m -order historical trajectories should be considered in the state prediction. Our experiment demonstrates the superior performance of HA3C over five state-of-the-art RL algorithms on MuJoCo control tasks. When it is hard to determine k with little prior knowledge, multi-head CNNs with different values of k can be utilized to learn the contexts in MDPs. This can be our future work.

486 REPRODUCIBILITY STATEMENT
487488 This paper fully discloses all the information needed to reproduce the main experimental results. The
489 experimental setting is in Appendix G. The experimental results can be reproduced by the updated
490 source code.
491492 REFERENCES
493494 Cameron Allen, Neev Parikh, Omer Gottesman, and George Konidaris. Learning markov state
495 abstractions for deep reinforcement learning. *Advances in Neural Information Processing Systems*,
496 34:8229–8241, 2021.497 Ankesh Anand, Evan Racah, Sherjil Ozair, Yoshua Bengio, Marc-Alexandre Côté, and R Devon
498 Hjelm. Unsupervised state representation learning in atari. *Advances in Neural Information
499 Processing Systems*, 32, 2019.
500501 Alexandr Andoni, Rina Panigrahy, Gregory Valiant, and Li Zhang. Learning polynomials with neural
502 networks. In *International Conference on Machine Learning*, pp. 1908–1916. PMLR, 2014.503 David Andre and Stuart J Russell. State abstraction for programmable reinforcement learning agents.
504 In *AAAI*, pp. 119–125, 2002.
505506 Benny Applebaum, Yuval Ishai, and Eyal Kushilevitz. Cryptography in nc^0 . *SIAM Journal on
507 Computing*, 36(4):845–888, 2006.508 Leemon Baird. Residual algorithms: Reinforcement learning with function approximation. In
509 *Machine Learning Proceedings 1995*, pp. 30–37. Elsevier, 1995.
510511 Maurice Stevenson Bartlett. *An introduction to stochastic processes*. University Press Cambridge,
512 1966.
513514 Aditya Bhatt, Daniel Palenicek, Boris Belousov, Max Argus, Artemij Amiranashvili, Thomas Brox,
515 and Jan Peters. Crossq: Batch normalization in deep reinforcement learning for greater sample
516 efficiency and simplicity. In *The Twelfth International Conference on Learning Representations*,
517 2024. URL <https://openreview.net/forum?id=PczQtTsTIX>.518 Monica Bianchini and Franco Scarselli. On the complexity of neural network classifiers: A compari-
519 son between shallow and deep architectures. *IEEE Transactions on Neural Networks and Learning
520 Systems*, 25(8):1553–1565, 2014.521 Yann Bouteiller, Simon Ramstedt, Giovanni Beltrame, Christopher Pal, and Jonathan Binas. Rein-
522 forcement learning with random delays. In *International Conference on Learning Representations*,
523 2020.
524525 Greg Brockman, Vicki Cheung, Ludwig Pettersson, Jonas Schneider, John Schulman, Jie Tang, and
526 Wojciech Zaremba. Openai gym. *arXiv preprint arXiv:1606.01540*, 2016.527 Jacob Buckman, Danijar Hafner, George Tucker, Eugene Brevdo, and Honglak Lee. Sample-efficient
528 reinforcement learning with stochastic ensemble value expansion. *Advances in Neural Information
529 Processing Systems*, 31, 2018.
530531 Miles Cranmer, Sam Greydanus, Stephan Hoyer, Peter Battaglia, David Spergel, and Shirley Ho.
532 Lagrangian neural networks. *arXiv preprint arXiv:2003.04630*, 2020.
533534 Peter Dayan. Improving generalization for temporal difference learning: The successor representation.
535 *Neural Computation*, 5(4):613–624, 1993.536 Esther Derman, Gal Dalal, and Shie Mannor. Acting in delayed environments with non-stationary
537 markov policies. In *International Conference on Learning Representations*, 2020.
538539 Esther Derman, Gal Dalal, and Shie Mannor. Acting in delayed environments with non-stationary
markov policies. *arXiv preprint arXiv:2101.11992*, 2021.

540 Richard C Dorf and Robert H Bishop. *Modern control systems*. Pearson, 2011.
 541

542 Simon S Du, Sham M Kakade, Ruosong Wang, and Lin F Yang. Is a good representation sufficient for
 543 sample efficient reinforcement learning? In *International Conference on Learning Representations*,
 544 2020.

545 Yan Duan, Xi Chen, Rein Houthooft, John Schulman, and Pieter Abbeel. Benchmarking deep
 546 reinforcement learning for continuous control. In *International Conference on Machine Learning*,
 547 volume 28, pp. 1329–1338, New York, USA, 2016.

548 EB Dynkin. *Markov processes*. Springer, 1965.

549

550 Kevin Esslinger, Robert Platt, and Christopher Amato. Deep transformer q-networks for partially
 551 observable reinforcement learning. In *NeurIPS 2022 Foundation Models for Decision Making*
 552 *Workshop*, 2022.

553

554 Eyal Even-Dar and Yishay Mansour. Learning rates for q-learning. *Journal of machine learning*
 555 *Research*, 5(Dec):1–25, 2003.

556 Ben Eysenbach, Xinyang Geng, Sergey Levine, and Russ R Salakhutdinov. Rewriting history with
 557 inverse rl: Hindsight inference for policy improvement. *Advances in Neural Information Processing*
 558 *Systems*, 33:14783–14795, 2020.

559

560 Scott Fujimoto, Herke Van Hoof, and David Meger. Addressing function approximation error in actor-
 561 critic methods. In *International Conference on Machine Learning*, volume 80, pp. 1587–1596,
 562 Stockholm, Sweden, 2018.

563 Scott Fujimoto, David Meger, and Doina Precup. An equivalence between loss functions and non-
 564 uniform sampling in experience replay. *Advances in Neural Information Processing Systems*, 33:
 565 14219–14230, 2020.

566

567 Scott Fujimoto, Wei-Di Chang, Edward J Smith, Shixiang Shane Gu, Doina Precup, and David Meger.
 568 For SALE: State-action representation learning for deep reinforcement learning. In *Thirty-seventh*
 569 *Conference on Neural Information Processing Systems*, 2023.

570

571 Carles Gelada, Saurabh Kumar, Jacob Buckman, Ofir Nachum, and Marc G Bellemare. Deepmdp:
 572 Learning continuous latent space models for representation learning. In *International Conference*
 573 *on Machine Learning*, pp. 2170–2179. PMLR, 2019.

574

575 Ruocheng Guo, Lu Cheng, Jundong Li, P Richard Hahn, and Huan Liu. A survey of learning causality
 576 with data: Problems and methods. *ACM Computing Surveys (CSUR)*, 53(4):1–37, 2020.

577

578 David Ha and Jürgen Schmidhuber. World models. *arXiv preprint arXiv:1803.10122*, 2018.

579

580 Tuomas Haarnoja, Aurick Zhou, Pieter Abbeel, and Sergey Levine. Soft actor-critic: Off-policy
 581 maximum entropy deep reinforcement learning with a stochastic actor. In *International Conference*
 582 *on Machine Learning*, volume 80, pp. 1861–1870, Stockholm, Sweden, 2018.

583

584 Danijar Hafner, Timothy Lillicrap, Jimmy Ba, and Mohammad Norouzi. Dream to control: Learning
 585 behaviors by latent imagination. In *International Conference on Learning Representations*, 2019a.

586

587 Danijar Hafner, Timothy Lillicrap, Ian Fischer, Ruben Villegas, David Ha, Honglak Lee, and James
 588 Davidson. Learning latent dynamics for planning from pixels. In *International Conference on*
 589 *Machine Learning*, pp. 2555–2565. PMLR, 2019b.

590

591 Assaf Hallak, Dotan Di Castro, and Shie Mannor. Contextual markov decision processes. *arXiv*
 592 *preprint arXiv:1502.02259*, 2015.

593

594 Matthew Hausknecht and Peter Stone. Deep recurrent q-learning for partially observable mdps. In
 595 *AAAI Fall Symposium Series*, 2015.

596

597 Peter Henderson, Riashat Islam, Philip Bachman, Joelle Pineau, Doina Precup, and David Meger.
 598 Deep reinforcement learning that matters. In *Proceedings of the AAAI Conference on Artificial*
 599 *Intelligence*, volume 32, 2018.

594 Sepp Hochreiter and Jürgen Schmidhuber. Long short-term memory. *Neural computation*, 9(8):
 595 1735–1780, 1997.

596

597 Peter J Huber. Robust estimation of a location parameter. In *Breakthroughs in Statistics: Methodology*
 598 and *Distribution*, pp. 492–518. Springer, 1992.

599 Julian Ibarz, Jie Tan, Chelsea Finn, Mrinal Kalakrishnan, Peter Pastor, and Sergey Levine. How to
 600 train your robot with deep reinforcement learning: lessons we have learned. *The International*
 601 *Journal of Robotics Research*, 40(4-5):698–721, 2021.

602

603 Tommi Jaakkola, Michael Jordan, and Satinder Singh. Convergence of stochastic iterative dynamic
 604 programming algorithms. *Advances in Neural Information Processing Systems*, 6, 1993.

605 Leslie Pack Kaelbling, Michael L Littman, and Andrew W Moore. Reinforcement learning: A survey.
 606 *Journal of Artificial Intelligence Research*, 4:237–285, 1996.

607

608 Markus Kalisch and Peter Bühlman. Estimating high-dimensional directed acyclic graphs with the
 609 pc-algorithm. *Journal of Machine Learning Research*, 8(3), 2007.

610 Konstantinos V Katsikopoulos and Sascha E Engelbrecht. Markov decision processes with delays
 611 and asynchronous cost collection. *IEEE Transactions on Automatic Control*, 48(4):568–574, 2003.

612

613 DP Kingma. Adam: a method for stochastic optimization. In *International Conference on Learning*
 614 *Representations*, 2015.

615 Arsenii Kuznetsov, Pavel Shvechikov, Alexander Grishin, and Dmitry Vetrov. Controlling overesti-
 616 mation bias with truncated mixture of continuous distributional quantile critics. In *International*
 617 *Conference on Machine Learning*, pp. 5556–5566. PMLR, 2020.

618

619 Lihong Li, Thomas J Walsh, and Michael L Littman. Towards a unified theory of state abstraction for
 620 mdps. In *AI&M*, 2006.

621

622 Timothy P Lillicrap, Jonathan J Hunt, Alexander Pritzel, Nicolas Heess, Tom Erez, Yuval Tassa,
 623 David Silver, and Daan Wierstra. Continuous control with deep reinforcement learning. In *International*
 624 *Conference on Learning Representations*, San Juan, Puerto Rico, 2016.

625

626 Guoqing Liu, Chuheng Zhang, Li Zhao, Tao Qin, Jinhua Zhu, Li Jian, Nenghai Yu, and Tie-Yan
 627 Liu. Return-based contrastive representation learning for reinforcement learning. In *International*
 628 *Conference on Learning Representations*, 2020.

629

630 Sultan Javed Majeed and Marcus Hutter. On q-learning convergence for non-markov decision
 631 processes. In *IJCAI*, volume 18, pp. 2546–2552, 2018.

632

633 Francisco S Melo. Convergence of q-learning: A simple proof. *Institute Of Systems and Robotics,*
 634 *Tech. Rep*, pp. 1–4, 2001.

635

636 Volodymyr Mnih, Koray Kavukcuoglu, David Silver, Andrei A Rusu, Joel Veness, Marc G Bellemare,
 637 Alex Graves, Martin Riedmiller, Andreas K Fidjeland, Georg Ostrovski, et al. Human-level control
 638 through deep reinforcement learning. *Nature*, 518(7540):529–533, 2015.

639

640 Volodymyr Mnih, Adria Puigdomenech Badia, Mehdi Mirza, Alex Graves, Timothy Lillicrap, Tim
 641 Harley, David Silver, and Koray Kavukcuoglu. Asynchronous methods for deep reinforcement
 642 learning. In *International Conference on Machine Learning*, pp. 1928–1937. PMLR, 2016.

643

644 Alfred Müller. Integral probability metrics and their generating classes of functions. *Advances in*
 645 *applied probability*, 29(2):429–443, 1997.

646

647 Jelle Munk, Jens Kober, and Robert Babuška. Learning state representation for deep actor-critic
 648 control. In *2016 IEEE 55th Conference on Decision and Control (CDC)*, pp. 4667–4673. IEEE,
 649 2016.

650

651 Chengzhuo Ni, Yaqi Duan, Munther Dahleh, Mengdi Wang, and Anru R Zhang. Learning good
 652 state and action representations for markov decision process via tensor decomposition. *Journal of*
 653 *Machine Learning Research*, 24(115):1–53, 2023.

648 Kei Ota, Tomoaki Oiki, Devesh Jha, Toshisada Mariyama, and Daniel Nikovski. Can increasing input
 649 dimensionality improve deep reinforcement learning? In *International Conference on Machine*
 650 *Learning*, pp. 7424–7433. PMLR, 2020.

651

652 Adam Paszke, Sam Gross, Francisco Massa, Adam Lerer, James Bradbury, Gregory Chanan, Trevor
 653 Killeen, Zeming Lin, Natalia Gimelshein, Luca Antiga, et al. Pytorch: An imperative style,
 654 high-performance deep learning library. *Advances in Neural Information Processing Systems*, 32,
 655 2019.

656

657 Gandharv Patil, Aditya Mahajan, and Doina Precup. On learning history-based policies for controlling
 658 markov decision processes. In *International Conference on Artificial Intelligence and Statistics*,
 659 pp. 3511–3519. PMLR, 2024.

660

661 Martin L Puterman. Markov decision processes. *Handbooks in operations research and management*
 662 *science*, 2:331–434, 1990.

663

664 Martin L Puterman. *Markov decision processes: discrete stochastic dynamic programming*. John
 665 Wiley & Sons, 2014.

666

667 Balaraman Ravindran. *An algebraic approach to abstraction in reinforcement learning*. University
 668 of Massachusetts Amherst, 2004.

669

670 Sahand Rezaei-Shoshtari, Rosie Zhao, Prakash Panangaden, David Meger, and Doina Precup. Con-
 671 tinuous mdp homomorphisms and homomorphic policy gradient. *Advances in Neural Information*
 672 *Processing Systems*, 35:20189–20204, 2022.

673

674 Ahmad EL Sallab, Mohammed Abdou, Etienne Perot, and Senthil Yogamani. Deep reinforcement
 675 learning framework for autonomous driving. *Electronic Imaging*, 2017(19):70–76, 2017.

676

677 John Schulman, Sergey Levine, Pieter Abbeel, Michael Jordan, and Philipp Moritz. Trust region
 678 policy optimization. In *International Conference on Machine Learning*, volume 37, pp. 1889–1897,
 679 Lille, France, 2015.

680

681 David Silver, Guy Lever, Nicolas Heess, Thomas Degris, Daan Wierstra, and Martin Riedmiller.
 682 Deterministic policy gradient algorithms. In *International Conference on Machine Learning*,
 683 volume 32, pp. 1387–1395, Beijing, China, 2014.

684

685 Shagun Sodhani, Franziska Meier, Joelle Pineau, and Amy Zhang. Block contextual mdps for
 686 continual learning. In *Learning for Dynamics and Control Conference*, pp. 608–623. PMLR, 2022.

687

688 David Sprunger and Bart Jacobs. The differential calculus of causal functions. *arXiv preprint*
 689 *arXiv:1904.10611*, 2019.

690

691 Richard S Sutton and Andrew G Barto. *Reinforcement learning: An introduction*. MIT press, 2018.

692

693 Yuval Tassa, Yotam Doron, Alistair Muldal, Tom Erez, Yazhe Li, Diego de Las Casas, David Budden,
 694 Abbas Abdolmaleki, Josh Merel, Andrew Lefrancq, et al. Deepmind control suite. *arXiv preprint*
 695 *arXiv:1801.00690*, 2018.

696

697 Yee Teh, Victor Bapst, Wojciech M Czarnecki, John Quan, James Kirkpatrick, Raia Hadsell, Nicolas
 698 Heess, and Razvan Pascanu. Distral: Robust multitask reinforcement learning. *Advances in Neural*
 699 *Information Processing Systems*, 30, 2017.

700

701 Emanuel Todorov, Tom Erez, and Yuval Tassa. Mujoco: A physics engine for model-based control.
 702 In *2012 IEEE/RSJ International Conference on Intelligent Robots and Systems*, pp. 5026–5033,
 703 Algarve, Portugal, 2012. IEEE.

704

705 Herke Van Hoof, Nutan Chen, Maximilian Karl, Patrick van der Smagt, and Jan Peters. Stable rein-
 706 forcement learning with autoencoders for tactile and visual data. In *2016 IEEE/RSJ International*
 707 *Conference on Intelligent Robots and Systems (IROS)*, pp. 3928–3934. IEEE, 2016.

708

709 Ashish Vaswani, Noam Shazeer, Niki Parmar, Jakob Uszkoreit, Llion Jones, Aidan N Gomez, Łukasz
 710 Kaiser, and Illia Polosukhin. Attention is all you need. *Advances in Neural Information Processing*
 711 *Systems*, 30, 2017.

702 Ronald J Williams. Simple statistical gradient-following algorithms for connectionist reinforcement
703 learning. *Machine Learning*, 8(3-4):229–256, 1992.
704

705 Mingxuan Ye, Yufei Kuang, Jie Wang, Rui Yang, Wengang Zhou, Houqiang Li, and Feng Wu.
706 State sequences prediction via fourier transform for representation learning. In *Thirty-seventh*
707 *Conference on Neural Information Processing Systems*, 2023.

708 Xue Ying. An overview of overfitting and its solutions. In *Journal of Physics: Conference Series*,
709 volume 1168, pp. 022022. IOP Publishing, 2019.
710

711 Amy Zhang, Rowan McAllister, Roberto Calandra, Yarin Gal, and Sergey Levine. Learning invariant
712 representations for reinforcement learning without reconstruction. In *International Conference on*
713 *Learning Representations*, 2021.

714
715
716
717
718
719
720
721
722
723
724
725
726
727
728
729
730
731
732
733
734
735
736
737
738
739
740
741
742
743
744
745
746
747
748
749
750
751
752
753
754
755

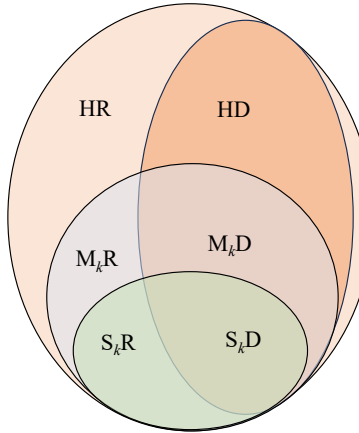
756 **A DIFFERENT POLICIES**
757

758 Time-related policies can be History-dependent (H) or k -order Markov (M_k) (Derman et al., 2020;
759 Puterman, 2014). Denote \mathcal{H}_t as the set of possible histories up to time step t . A history-dependent
760 policy $\pi = \{d_t | t = 0, 1, \dots\}$ at t maps histories to actions as $d_t : \mathcal{H}_t \mapsto \mathcal{A}$. A k -order Markov policy
761 $\pi = \{d_t | t = 0, 1, \dots\}$ at t maps k -order state transition trajectories to actions as $d_t : \mathcal{S}_{k,t} \mapsto \mathcal{A}$. A
762 k -order stationary (S_k) policy is unrelated to time as $\pi : \mathcal{S}_{k,:} \mapsto \mathcal{A}$. In general, a randomized (R)
763 policy selects the actions by a probability distribution as $\pi(\mathbf{a}|*)$. π is a deterministic (D) policy if
764 and only if $\pi(\mathbf{a}|*) \in \{0, 1\}$. Based on the above analysis, we can obtain History-dependent Random
765 (HR) policies, History-dependent Deterministic (HD) policies, k -order Markov Random ($M_k R$)
766 policies, k -order Markov Deterministic ($M_k D$) policies, k -order Stationary Random ($S_k R$) policies,
767 and k -order Stationary Deterministic ($S_k D$) policies.

768 The above policies are summarized in Table 2. The relationships among them are demonstrated in
769 Fig. 9. It is noteworthy that sometimes historical actions will be considered in decision-making. In
770 this case, without loss of generality, a historical state $\mathbf{s}_{i|i \leq t-1}$ can be updated by $\mathbf{s}_i \leftarrow \mathbf{s}_i \cup \mathbf{a}_i$.

772 **Table 2: Different types of policies.**

774 Policy	775 Abbreviation	776 Action
775 History-dependent Random	776 HR	$777 \mathbf{a}_t \sim d_t(\mathbf{s}_{0,t}), d_t \in \pi$
776 History-dependent Deterministic	777 HD	$778 \mathbf{a}_t = d_t(\mathbf{s}_{0,t}), d_t \in \pi$
777 k -order Markov Random	778 $M_k R$	$779 \mathbf{a}_t \sim d_t(\mathbf{s}_{k-t+1,t}), d_t \in \pi$
778 k -order Markov Deterministic	779 $M_k D$	$780 \mathbf{a}_t = d_t(\mathbf{s}_{k-t+1,t}), d_t \in \pi$
779 k -order Stationary Random	780 $S_k R$	$781 \mathbf{a}_t \sim \pi(\mathbf{s}_{k-t+1,t})$
780 k -order Stationary Deterministic	781 $S_k D$	$782 \mathbf{a}_t = \pi(\mathbf{s}_{k-t+1,t})$

798 **Figure 9: The relations among different policies.**

810

811

812

813

814

815

816

817

818

819

820

B THE TOY EXPERIENCE ON FIBONACCI SEQUENCE

We design a toy experience on Fibonacci sequence for didactic purposes as follows. Given a finite Fibonacci sequence (Fseq), $l_0 = 1, l_1 = 1, l_2 = 2, l_3 = 3, l_4 = 5, \dots$, we define a Markov decision process as:

1. A state s is defined by the corresponding item l and the initial state is defined by $s_0 = l_1$.
2. The action space of a is the natural numbers.
3. Define s' as the next state of s and l' as the next item of l . If the agent can accurately predict l' at l , i.e., $a = l'$, the agent will move forward in the sequence, i.e., $s' = l'$, otherwise, the agent will remain stationary, i.e., $s' = l$.
4. If $s' = l'$, we set reward $r = 1$, Otherwise, $r = 0$. This reward is designed to make the agent move forward in the sequence.

We respectively train two policy networks, A and B , to solve the above MDP. At step t , the input of A is s_{t-1}, s_t (considering historical information) but the input of B is only s_t (without considering historical information). The Table 3 shows the cumulative rewards of training and testing the two policy networks with different orders of Fseqs. $A(i)$ means training A with i -order Fseq.

As we can see, by training with historical information, policy network A can make the agent move forward in the Fseq of a higher order than that of the training Fseq, i.e., A can learn the causal relationships in the Fseq. However, without historical information in training, policy network B can only make the agent move forward in the Fseq of a lower order than that of the training Fseq, i.e., B cannot learn the causal relationships in the Fseq but solve the problem by brute-force approximation. This experience shows that augmenting the states with their historical information can simplify the complex causal relationships in MDPs and thus improve the sample efficiency of DRL.

C TWO EXAMPLES OF IMPROVING SAMPLE EFFICIENCY IN MDPs BY HISTORICAL AUGMENTATION

C.1 POLYNOMIAL EXAMPLE

Define a sequence as follows: 1) $|\beta_0| \neq 1$; 2) If $i > 1$, then $\beta_{i+1} = \beta_i^2$.

Based on the sequence above, we can define an MDP $\mathbb{M} = \langle \mathcal{S}, \mathcal{A}, R, \mathbf{P}, \gamma \rangle$. At time step t , state $s_t = [\beta_t, \beta_{t+2}]^\top$ and action a_t is computed by a linear function $f(\cdot)$ on state s_t or augmented state $s_{k,t}$. Without considering historical information, reward r_t is defined as

$$r_t = -|f(s_t) - (\beta_t + \sqrt{\beta_{t+2}} + \beta_{t+2})| = -|\mathbf{w}s_t + b - (\beta_t + \sqrt{\beta_{t+2}} + \beta_{t+2})|, \quad (6)$$

where \mathbf{w} is a two-dimensional vector and b is a constant. In transition model \mathbf{P} , s_0 can be defined as $[\beta_0, \beta_2]^\top$ and s_{t+1} can be computed by s_t as

$$s_{t+1} = [\beta_t^2, \beta_{t+2}^2]^\top = s_t \odot s_t, \quad (7)$$

where \odot is Hadamard product. $\gamma = 0.99$.

From equation 6 and equation 7, it is easy to see that \mathbb{M} satisfies the Markov assumption of MDPs. To maximize the discounted cumulative reward in \mathbb{M} , we should minimize

$$\arg \min_{\mathbf{w}, b} \|f(s_t) - (\beta_t + \sqrt{\beta_{t+2}} + \beta_{t+2})\|_2 = \arg \min_{\mathbf{w}, b} \|\mathbf{w}s_t + b - (\beta_t^2 + \sqrt{\beta_{t+2}} + \beta_{t+2})\|_2 \quad (8)$$

at each time step t . However, it is hard to minimize equation 8 by $f(s_t)$, which is a linear model on s_t .

864 The above problem can be solved by the historical augmentation of s_t . When considering the
 865 historical augmentation of s_t , $f(*)$ on $s_{2,t}$ can be defined as
 866

$$867 \quad f(s_{2,t}) = \mathbf{w}_0 s_t + \mathbf{w}_1 s_{t-1} + b.$$

868 Instead of minimizing equation 8, we can minimize
 869

$$870 \quad \arg \min_{\mathbf{w}_0, \mathbf{w}_1, b} \|f(s_{2,t}) - (\beta_t + \sqrt{\beta_{t+2}} + \beta_{t+2})\|_2$$

$$871 \quad = \arg \min_{\mathbf{w}_0, \mathbf{w}_1, b} \|\mathbf{w}_0 s_t + \mathbf{w}_1 s_{t-1} + b - (\beta_t^2 + \sqrt{\beta_{t+2}} + \beta_{t+2})\|_2.$$

872 Let $\mathbf{w}_0 = [1, 1]$, $\mathbf{w}_1 = [0, 1]$, and $b = 0$. From $\beta_{t+1} = \sqrt{\beta_{t+2}}$, we have
 873

$$874 \quad \|\mathbf{w}_0 s_t + \mathbf{w}_1 s_{t-1} + b - (\beta_t + \sqrt{\beta_{t+2}} + \beta_{t+2})\|_2$$

$$875 \quad = \|\mathbf{w}_0 s_t + \mathbf{w}_1 s_{t-1} + b - (\beta_t + \beta_{t+1} + \beta_{t+2})\|_2$$

$$876 \quad = \|([1, 1][\beta_t, \beta_{t+2}]^\top + [0, 1][\beta_{t-1}, \beta_{t+1}]^\top - (\beta_t + \beta_{t+1} + \beta_{t+2}))\|_2$$

$$877 \quad = 0.$$

878 In this case, the cumulative reward in \mathbb{M} can be maximized.
 879

880 C.2 PHYSICAL EXAMPLE

881 Newton's second law of motion states that the acceleration of an object is directly proportional to the
 882 net force acting on it and inversely proportional to its mass, i.e., $\vec{\alpha} = \vec{F}/m$, where \vec{F} is the force, m
 883 is the mass, and $\vec{\alpha}$ is the acceleration.
 884

885 Based on Newton's second law of motion, given an object with an initial speed \vec{v}_0 in a physical
 886 model Ω , with the assumption that the forces on the object are only related to Ω , we provide a formal
 887 definition of the MDP example as follows. State s_t is defined as $\{m, \vec{v}_t, \Omega\}$. Action a_t is used to
 888 predict the future speed \vec{v}_{t+1} . The basic state transition is
 889

$$890 \quad s_{t+1} = \{m, \vec{v}_t + \vec{\alpha}_t \Delta t, \Omega\} = \{m, \vec{v}_t + \frac{\vec{F}_t \Delta t}{m}, \Omega\} = \{m, \vec{v}_t + \frac{\mathcal{F}(\Omega) \Delta t}{m}, \Omega\}$$

891 where \mathcal{F} is the force analysis function. As we can see, the causes of the acceleration $\vec{\alpha}_t$ are only m
 892 and $\mathcal{F}(\Omega)$. However, \mathcal{F} is usually hard to approximate. Fortunately, there is historical context of $\vec{\alpha}$
 893 as $\vec{\alpha} = d\vec{v}/dt$. When there is a high sampling frequency of the states, the historical speed can be
 894 regarded as the **prompt** for quickly approximating the acceleration of the object. Then the future
 895 speed can be accurately predicted. In the above MDP, s_{t+1} is only generated by s_t and a_t , but there
 896 can be some historical context in this MDP.
 897

900 D CONNECTED TO RELATED WORK

901 D.1 CONNECTED TO HMDPs

902 In HMDPs, the probability distributions of the reward and next state depend not only on the current
 903 state and action but also on the historical states and actions. For a k -order HMDPs, we have
 904

$$905 \quad P\{s_{t+1} = s', r_t = r | s_0, a_0, r_0, \dots, s_t, a_t\} = P\{s_{t+1} = s', r_t = r | s_{t-k+1}, a_{t-k+1}, \dots, s_t, a_t\}.$$

906 The causal diagram of HMDP is presented in Fig. 10(a). Our approach optimizes the policy by a
 907 simplified HMDP model in which the probability distributions of the reward and next state depend on
 908 the current state-action pair and compressed historical trajectory as
 909

$$910 \quad P\{s_{t+1} = s', r_t = r | s_0, a_0, r_0, \dots, s_t, a_t\} = P\{s_{t+1} = s', r_t = r | DR(s_{t-1, k-1}), \dots, s_t, a_t\}.$$

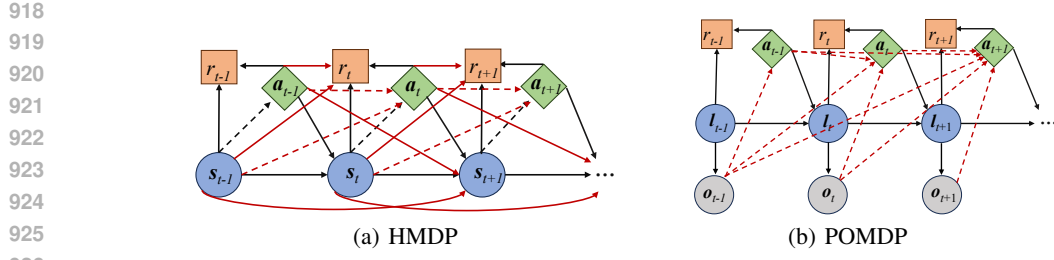


Figure 10: Causal diagram of HMDPs and POMDPs.

D.2 CONNECTED TO POMDPs

In POMDPs, the states are partially observable. Define the partially observable state at time step t as l_t and the observable part of l_t as o_t . The causal diagram of POMDPs is shown in Fig. 10(b). Under the faithfulness assumption, o_t and o_{t+k} are mutually dependent conditional on $\forall k > 1$, $\{o_i, a_i\}_{t < i < t+k}$ (Kalisch & Bühlman, 2007). Therefore, in a POMDP, the optimal policy π at time step t should consider not only o_t but also the historical information $\{o_i, a_i\}_{0 \leq i < t}$. When k is large, long-length rollout estimation is needed in POMDPs.

RL algorithms of world models, such as Dream, model the sequential decision-making as a POMDP (Ha & Schmidhuber, 2018; Hafner et al., 2019a). They usually encode the historical information at t by an encoder f^t to construct s_{t+1} as

$$s_{t+1} = f^t(o_t, a_t, \dots, f^1(o_1, a_1, f^0(o_0, a_0))).$$

When t is large, some partially observable states will be encoded many times, leading to the loss of some important discriminative information.

Compared with POMDP-based RL algorithms, our HA3C can better adjust the considered steps in history according to the actual task and thus effectively find the optimal policy in history-based sequential decision-making.

D.3 CONNECTED TO STATE ABSTRACTION

State abstraction aims to reduce ground MDPs with large state spaces to abstract MDPs with smaller state spaces by aggregating states according to some notion of equality or similarity (Bartlett, 1966). Through abstraction, intelligent agents may need to consider only the salient distinguishing information of their environments. Given an abstraction function as $F : \mathcal{S} \rightarrow \overline{\mathcal{S}}$, we can define the abstract version of MDP \mathbb{M} as $\overline{\mathbb{M}} = \langle \overline{\mathcal{S}}, \mathcal{A}, \overline{R}, \overline{P}, \gamma \rangle$. A Q -irrelevance abstraction function F^Q is that for any action a , $F^Q(s) = F^Q(s')$ implies $Q(s, a) = Q(s', a)$. Then we have the following theorem.

Theorem D.1. Define an MDP as $\mathbb{M}_k = \langle \mathcal{S}_{k,:}, \mathcal{A}, R, \mathbf{P}_k, \gamma \rangle$. Under the conditions 1), 2), and 3) in Theorem 4.2, encoder f is a Q -irrelevance abstraction on $\mathcal{S}_{k,:}$.

Theorem D.1 illustrates that our representation learning can be seen as the Q -irrelevance abstraction of the historically augmented states. The proof of this theorem is given in Appendix E.

E THEORETICAL ANALYSIS

E.1 PROOF OF THEOREM 4.1

Now we give the proof to Theorem 4.1. The different types of policies in this proof are summarized in Table 2. The relationships between these policies are shown in Fig. 9.

Based on the Markov assumption of MDPs, we have

$$\begin{aligned} & P\{s_{t+1} = s', r_t = r | s_0, a_0, r_0, \dots, s_t, a_t\} \\ &= P\{s_{t+1} = s', r_t = r | s_{t-k+1:t}, a_t\} \\ &= P\{s_{t+1} = s', r_t = r | s_t, a_t\}. \end{aligned} \tag{9}$$

972 For any $\pi \in HR$, we can define $V_\pi(\mathbf{h}_t)$ by
 973

$$974 \quad V^\pi(\mathbf{h}_t) = \mathbb{E}^\pi \left[\sum_{i=t}^{+\infty} \gamma^i R(\mathbf{h}_{t+i}, \mathbf{a}_{t+i}) \right].$$

975 From Fig. 9, we have $S_k D \in M_k D \in M_k R \in HR$. In view of equation 9, we see for all t that
 976

$$977 \quad \sup_{\pi \in HR} V^\pi(\mathbf{h}_t) = \sup_{\pi \in S_k D} V^\pi(\mathbf{s}_{k,t}).$$

978 First, for all t , we demonstrate that
 979

$$980 \quad \sup_{\pi \in HR} V^\pi(\mathbf{h}_t) = \sup_{\pi \in M_k R} V^\pi(\mathbf{s}_{k,t}). \quad (10)$$

981 This is a direct result of Theorem E.1. The proof of this theorem is presented in E.1.1.
 982

983 **Theorem E.1.** *Let $\pi = \{d_t | t = 0, 1, \dots\} \in HR$. Then $\forall \mathbf{s}_{k,:} \in \mathcal{S}_{k,:}$, based on equation 9, there exists
 984 a policy $\pi' = \{d'_t | t = 0, 1, \dots\} \in M_k R$ satisfying*
 985

$$986 \quad p^\pi(\mathbf{a}_{t+i} = \mathbf{a}', \mathbf{s}_{k,t+i} = \mathbf{s}'_{k,:} | \mathbf{s}_{k,t} = \mathbf{s}_{k,:}) = p^{\pi'}(\mathbf{a}_{t+i} = \mathbf{a}', \mathbf{s}_{k,t+i} = \mathbf{s}'_{k,:} | \mathbf{s}_{k,t} = \mathbf{s}_{k,:}),$$

987 where $p^\pi(*)$ denotes the probability of $*$ provided that the agent follows policy π .
 988

989 Then Theorem E.2 illustrates that the value functions of $\pi \in M_k D$ and $\pi \in M_k R$ have the same
 990 upper bound. The proof of this theorem is demonstrated in E.1.2.
 991

992 **Theorem E.2.** *If a bounded function V on $\mathcal{S}_{k,:}$ satisfies the optimal Bellman equation that*
 993

$$994 \quad V(\mathbf{s}_{k,t}) = \sup_{\mathbf{a} \in \mathcal{A}} \left\{ R(\mathbf{s}_{k,t}, \mathbf{a}) + \gamma \int_{\mathcal{S}_{k,:}} V(\mathbf{s}_{k,t+1} | \mathbf{s}_{t+1} = \mathbf{s}') p(\mathbf{s}' | \mathbf{s}_{k,t}, \mathbf{a}) d\mathbf{s}'_{k,:} \right\},$$

995 then
 996

$$997 \quad \sup_{\pi \in M_k D} V^\pi(\mathbf{s}_{k,t}) = \sup_{\pi \in M_k R} V^\pi(\mathbf{s}_{k,t}).$$

998 Finally, based on equation 9, for all $\mathbf{s}_{k,:} \in \mathcal{S}_{k,:}$, if $\mathbf{s}_{k,t} = \mathbf{s}_{k,:}$, then
 999

$$1000 \quad \sup_{\mathbf{a} \in \mathcal{A}} V(\mathbf{s}_{k,t}) = \sup_{\mathbf{a} \in \mathcal{A}} V(\mathbf{s}_{k,:}). \quad (11)$$

1001 Let $\mathbf{a} = \pi(\mathbf{s}_{k,:})$, where $\pi \in S_k D$. It follows that
 1002

$$1003 \quad \sup_{\pi \in S_k D} V^\pi(\mathbf{s}_{k,:}) = \sup_{\pi \in M_k D} V^\pi(\mathbf{s}_{k,t}). \quad (12)$$

1004 Under equation 10, equation 11 and equation 12, $\forall t$, if $\mathbf{s}_{k,t} = \mathbf{s}_{k,:}$, then
 1005

$$1006 \quad \sup_{\pi \in HR} V^\pi(\mathbf{h}_t) = \sup_{\pi \in M_k R} V^\pi(\mathbf{s}_{k,t}) = \sup_{\pi \in M_k D} V^\pi(\mathbf{s}_{k,t}) = \sup_{\pi \in S_k D} V^\pi(\mathbf{s}_{k,:}).$$

1007 E.1.1 PROOF OF THEOREM E.1

1008 We assume that Theorem E.1 holds for $i = 1, 2, 3, \dots, n-1$. Given a policy $\pi \in HR$, based
 1009 on equation 9, we see that there exists a policy $\pi' \in M_k R$ satisfying
 1010

$$1011 \quad \begin{aligned} & p^\pi(\mathbf{s}_{k,t+i} = \mathbf{s}''_{k,:} | \mathbf{s}_{k,t} = \mathbf{s}_{k,:}) \\ &= \int_{\mathcal{S}_{k,:}} \int_{\mathcal{A}} p^\pi(\mathbf{s}_{k,t+i-1} = \mathbf{s}'_{k,:}, \mathbf{a}_{t+i-1} = \mathbf{a}' | \mathbf{s}_{k,t} = \mathbf{s}_{k,:}) p(\mathbf{s}'' | \mathbf{s}'_{k,:}, \mathbf{a}') d\mathbf{a}' d\mathbf{s}'_{k,:} \\ &= \int_{\mathcal{S}_{k,:}} \int_{\mathcal{A}} p^{\pi'}(\mathbf{s}_{k,t+i-1} = \mathbf{s}'_{k,:}, \mathbf{a}_{t+i-1} = \mathbf{a}' | \mathbf{s}_{k,t} = \mathbf{s}_{k,:}) p(\mathbf{s}'' | \mathbf{s}'_{k,:}, \mathbf{a}') d\mathbf{a}' d\mathbf{s}'_{k,:} \\ &= p^{\pi'}(\mathbf{s}_{k,t+i} = \mathbf{s}''_{k,:} | \mathbf{s}_{k,t} = \mathbf{s}_{k,:}). \end{aligned}$$

1018 The above equality follows from the induction hypothesis. The π' also can satisfy
 1019

$$1020 \quad p^{\pi'}(\mathbf{a}_{t+i} = \mathbf{a}' | \mathbf{s}_{k,t+i} = \mathbf{s}'_{k,:}) = p^\pi(\mathbf{a}_{t+i} = \mathbf{a}' | \mathbf{s}_{k,t+i} = \mathbf{s}'_{k,:}).$$

1021 Therefore,
 1022

$$1023 \quad \begin{aligned} & p^{\pi'}(\mathbf{a}_{t+i} = \mathbf{a}', \mathbf{s}_{k,t+i} = \mathbf{s}'_{k,:} | \mathbf{s}_{k,t} = \mathbf{s}_{k,:}) \\ &= p^{\pi'}(\mathbf{a}_{t+i} = \mathbf{a}' | \mathbf{s}_{k,t+i} = \mathbf{s}'_{k,:}) p^{\pi'}(\mathbf{s}_{k,t+i} = \mathbf{s}'_{k,:} | \mathbf{s}_{k,t} = \mathbf{s}_{k,:}) \\ &= p^\pi(\mathbf{a}_{t+i} = \mathbf{a}' | \mathbf{s}_{k,t+i} = \mathbf{s}'_{k,:}) p^\pi(\mathbf{s}_{k,t+i} = \mathbf{s}'_{k,:} | \mathbf{s}_{k,t} = \mathbf{s}_{k,:}) \\ &= p^\pi(\mathbf{a}_{t+i} = \mathbf{a}', \mathbf{s}_{k,t+i} = \mathbf{s}'_{k,:} | \mathbf{s}_{k,t} = \mathbf{s}_{k,:}). \end{aligned}$$

1026 E.1.2 PROOF OF THEOREM E.2
10271028 In view of $M_k D \in M_k R$, we have

1029
$$\sup_{\pi \in M_k D} V^\pi(s_{k,t}) \leq \sup_{\pi \in M_k R} V^\pi(s_{k,t}). \quad (13)$$

1030

1031 It follows that

1032
$$\begin{aligned} 1033 \sup_{\mathbf{a} \in \mathcal{A}} & \left\{ R(s_{k,t}, \mathbf{a}) + \gamma \int_{\mathcal{S}_{k,:}} V(s_{k,t+1} | s_{k,t+1} = \mathbf{s}') p(\mathbf{s}' | s_{k,t}, \mathbf{a}) d\mathbf{s}' \right\} \\ 1034 \\ 1035 \geq & \int_{\mathcal{A}} p(d_t(s_{k,t}) = \mathbf{a}) \left[R(s_{k,t}, \mathbf{a}) + \gamma \int_{\mathcal{S}_{k,:}} V(s_{k,t+1} | s_{t+1} = \mathbf{s}') p(\mathbf{s}' | s_{k,t}, \mathbf{a}) d\mathbf{s}' \right] d\mathbf{a}, \\ 1036 \\ 1037 \end{aligned}$$

1038 where $d_t \in M_k R$. Thus

1039
$$\sup_{\pi \in M_k D} V^\pi(s_{k,t}) \geq \sup_{\pi \in M_k R} V^\pi(s_{k,t}). \quad (14)$$

1040

1041 Combining equation 13 and equation 14, we have

1042
$$\sup_{\pi \in M_k D} V^\pi(s_{k,t}) = \sup_{\pi \in M_k R} V^\pi(s_{k,t}).$$

1043

1044 E.2 PROOF OF THEOREM 4.2
10451046 To prove Theorem 4.2, we give the proof of Theorem D.1 first. Under the condition 1) of Theorem 4.2, one sees that there are only two independent variables $s_{k,:}$ and \mathbf{a} . Under the Markov assumption and the condition 2) of Theorem 4.2, we have

1047
$$P\{s_{k,t+1} = s'_{k,:} | s_0, \mathbf{a}_0, r_0, \dots, s_t, \mathbf{a}_t\} = P\{s_{k,t+1} = s'_{k,:} | \mathbf{z}^{s_{k,t}}, \mathbf{a}_t\}. \quad (15)$$

1048

1049 Then, under the condition 3) of Theorem 4.2, we have

1050
$$\begin{aligned} 1051 P\{\mathbf{z}^{s_{k,t+1}} = \mathbf{z}^{s'_{k,:}} | s_{k,t}, \mathbf{a}_t\} & \doteq P\{\mathbf{z}^{s_{k,t+1}} = \mathbf{z}^{s'_{k,:}} | \mathbf{z}^{s_{k,t}}, \mathbf{a}_t\} \\ 1052 & = P\{\mathbf{z}^{s_{k,t+1}} = \mathbf{z}^{s'_{k,:}} | g(f(s_{k,t}), \mathbf{a}_t)\} \\ 1053 & = P\{\mathbf{z}^{s_{k,t+1}} = \mathbf{z}^{s'_{k,:}} | g(\mathbf{z}^{s_{k,t}}, \mathbf{a}_t)\} \\ 1054 & = P\{\mathbf{z}^{s_{k,t+1}} = \mathbf{z}^{s'_{k,:}} | \mathbf{z}^{s_{k,t}}, \mathbf{a}_t\}. \\ 1055 \\ 1056 \\ 1057 \\ 1058 \\ 1059 \end{aligned} \quad (16)$$

1060 Define an MDP as $\mathbb{M}_k = \langle \mathcal{S}_{k,:}, \mathcal{A}, R, \mathbf{P}_k, \gamma \rangle$. From equation 15 and equation 16, we obtain
1061

1062
$$\mathbf{z}^{s_{k,:}} = \mathbf{z}^{s'_{k,:}} \rightarrow Q(s_{k,:}, \mathbf{a}) = Q(s'_{k,:}, \mathbf{a})$$

1063

1064 Because $\mathbf{z}^{s_{k,:}} = f(s_{k,:})$, we see that encoder f is a Q -irrelevance abstraction on $s_{k,:}$.
10651066 Define an abstracted MDP of \mathbb{M}_k as $\overline{\mathbb{M}}_k = \langle \mathcal{Z}, \mathcal{A}, R, \mathbf{P}_k, \gamma \rangle$, where \mathcal{Z} is the encoded space of $\mathcal{S}_{k,:}$.
1067 Operator B_μ can be written as
1068

1069
$$B_\mu \hat{Q}(\mathbf{z}^{s_{k,:}}, \mathbf{a}) = R(\mathbf{z}^{s_{k,:}}, \mathbf{a}) + \max_\mu \gamma \int_{\mathcal{Z}} \hat{Q}(\mathbf{z}^{s_{k,:}}, \mu(\mathbf{z}^{s_{k,:}})) p(\mathbf{z}^{s'_{k,:}} | \mathbf{z}^{s_{k,:}}, \mathbf{a}) d\mathbf{z}^{s'_{k,:}}.$$

1070

1071 Now we provide a proof (sketch) to Theorem 4.2. Since the optimality of μ follows from the optimal
1072 actions as well as their Q -values are preserved after abstraction, we see that B is a contraction in the
1073 sup-norm and the optimal Q -function \hat{Q}^* is the unique fixed point of B . Thus we can finally find the
1074 optimal policy μ^* by B_μ (Melo, 2001). When the agent estimates the optimal Q -function based on
1075 experience, we have the following update rule in each time step T by Lemma E.3 (Jaakkola et al.,
1076 1993; Melo, 2001).

1077
$$\hat{Q}_{t+1}(\mathbf{z}^{s_{k,t}}, \mathbf{a}_t) = \hat{Q}_t(\mathbf{z}^{s_{k,t}}, \mathbf{a}_t) + \alpha_t (r_t + \gamma \max_\mu \hat{Q}_t(\mathbf{z}^{s_{k,t+1}}, \mu(\mathbf{z}^{s_{k,t+1}})) - \hat{Q}_t(\mathbf{z}^{s_{k,t}}, \mathbf{a}_t)).$$

1078

1079 \hat{Q}_t converges to Q^* as long as

1080
$$\sum_{t=0}^{\infty} \alpha_t = \infty, \quad \sum_{t=0}^{\infty} \alpha_t^2 < \infty.$$

1081

1080

Lemma E.3. *The random process $\{\Delta_t\}$ taking values in \mathbb{R}^n and defined as*

$$\Delta_{t+1}(\mathbf{y}) = (1 - \alpha_t)\Delta_t(\mathbf{y}) + \alpha_t F_t(\mathbf{y})$$

1081

converges to zero under the following assumptions:

1082

1) $\sum_{t=0}^{\infty} \alpha_t = \infty$ and $\sum_{t=0}^{\infty} \alpha_t^2 < \infty$,

1083

2) $\mathbb{E}[|F_t(\mathbf{y})| \mathcal{F}_t] \leq \gamma \|\Delta_t\|_w$ with $\gamma < 1$, and

1084

3) $\text{Var}[F_t(\mathbf{y}) | \mathcal{F}_t] \leq C(1 + \|\Delta_t\|_w^2)$ for $C > 0$,

1085

where $\mathcal{F} = \{\Delta_t, \Delta_{t-1}, \dots, F_{t-1}, \dots, \alpha_{t-1}, \dots\}$ strands for the past at step t and $\|\cdot\|_w$ refers to some weighted maximum norm.

1086

1087

1088

E.3 APPROXIMATION ERROR ANALYSIS

1089

1090

1091

Define the value function in \mathcal{Z} as \hat{V} . The bound of the approximation error between the transition probabilities in space $\mathcal{S}_{k,:}$, and \mathcal{Z} based on the optimal value function \hat{V}^* can be defined as (Müller, 1997)

1092

1093

1094

$$\max_{\mathbf{s}_{k,:}, \mathbf{a}} \left| \int_{\mathcal{S}_{k,:}} \hat{V}^*(\mathbf{z}^{\mathbf{s}'_{k,:}}) p(\mathbf{s}'_{k,:} | \mathbf{s}_{k,:}, \mathbf{a}) d\mathbf{s}'_{k,:} - \int_{\mathcal{Z}} \hat{V}^*(\mathbf{z}^{\mathbf{s}'_{k,:}}) p(\mathbf{z}^{\mathbf{s}'_{k,:}} | \mathbf{z}^{\mathbf{s}_{k,:}}, \mathbf{a}) d\mathbf{z}^{\mathbf{s}'_{k,:}} \right| = \delta.$$

1095

Based on δ , we analyze the approximation error in Theorem E.4.

1096

Theorem E.4. *The worst-case difference between $V^\mu(\mathbf{z}^{\mathbf{s}_{k,:}})$ and optimal value function $V^*(\mathbf{s})$ is bounded as:*

1097

1098

1099

$$\|V^*(\mathbf{s}) - \hat{V}^*(\mathbf{z}^{\mathbf{s}_{k,:}})\|_\infty \leq \frac{\gamma\delta}{1-\gamma}.$$

1100

1101

1102

We provide the proof to the above theorem as follows. Based on the Markov assumption of MDPs, we have

1103

$$\|V^*(\mathbf{s}) - \hat{V}^*(\mathbf{z}^{\mathbf{s}_{k,:}})\|_\infty = \|V^*(\mathbf{s}_{k,:}) - \hat{V}^*(\mathbf{z}^{\mathbf{s}_{k,:}})\|_\infty.$$

1104

Now we prove that

1105

1106

1107

$$\|V^*(\mathbf{s}_{k,:}) - \hat{V}^*(\mathbf{z}^{\mathbf{s}_{k,:}})\|_\infty \leq \frac{\gamma\delta}{1-\gamma}. \quad (17)$$

1108

In view of $R(\mathbf{s}, \mathbf{a}) = R(\mathbf{s}_{k,:}, \mathbf{a}) = R(\mathbf{z}^{\mathbf{s}_{k,:}}, \mathbf{a})$ in the value function approximation, we have

1109

1110

1111

1112

1113

1114

1115

1116

1117

1118

1119

1120

1121

1122

1123

1124

$$\|V^*(\mathbf{s}_{k,:}) - \hat{V}^*(\mathbf{z}^{\mathbf{s}_{k,:}})\|_\infty$$

$$\leq \max_{\mathbf{s}_{k,:}, \mathbf{a}} \|Q^*(\mathbf{s}_{k,:}, \mathbf{a}) - \hat{Q}^*(\mathbf{z}^{\mathbf{s}_{k,:}}, \mathbf{a})\|$$

$$= \max_{\mathbf{s}_{k,:}, \mathbf{a}} \left| R(\mathbf{s}_{k,:}, \mathbf{a}) + \gamma \int_{\mathcal{S}_{k,:}} V^*(\mathbf{s}'_{k,:}) p(\mathbf{s}'_{k,:} | \mathbf{s}_{k,:}, \mathbf{a}) d\mathbf{s}'_{k,:} \right.$$

$$- \left. R(\mathbf{z}^{\mathbf{s}_{k,:}}, \mathbf{a}) - \gamma \int_{\mathcal{Z}} \hat{V}^*(\mathbf{z}^{\mathbf{s}'_{k,:}}) p(\mathbf{z}^{\mathbf{s}'_{k,:}} | \mathbf{z}^{\mathbf{s}_{k,:}}, \mathbf{a}) d\mathbf{z}^{\mathbf{s}'_{k,:}} \right|$$

$$\leq \gamma \max_{\mathbf{s}_{k,:}, \mathbf{a}} \left| \int_{\mathcal{S}_{k,:}} V^*(\mathbf{s}'_{k,:}) p(\mathbf{s}'_{k,:} | \mathbf{s}_{k,:}, \mathbf{a}) d\mathbf{s}'_{k,:} - \hat{V}^*(\mathbf{z}^{\mathbf{s}'_{k,:}}) p(\mathbf{z}^{\mathbf{s}'_{k,:}} | \mathbf{z}^{\mathbf{s}_{k,:}}, \mathbf{a}) d\mathbf{z}^{\mathbf{s}'_{k,:}} \right|$$

$$+ \gamma \max_{\mathbf{s}_{k,:}, \mathbf{a}} \left| \int_{\mathcal{S}_{k,:}} \hat{V}^*(\mathbf{z}^{\mathbf{s}'_{k,:}}) p(\mathbf{s}'_{k,:} | \mathbf{s}_{k,:}, \mathbf{a}) d\mathbf{s}'_{k,:} - \int_{\mathcal{Z}} \hat{V}^*(\mathbf{z}^{\mathbf{s}'_{k,:}}) p(\mathbf{z}^{\mathbf{s}'_{k,:}} | \mathbf{z}^{\mathbf{s}_{k,:}}, \mathbf{a}) d\mathbf{z}^{\mathbf{s}'_{k,:}} \right|$$

$$\leq \gamma \left(\|V^*(\mathbf{s}_{k,:}) - \hat{V}^*(\mathbf{z}^{\mathbf{s}_{k,:}})\|_\infty + \delta \right).$$

1125

This proves equation 17. Thus Theorem E.4 holds.

1126

1127

E.4 SAMPLE COMPLEXITY ANALYSIS

1128

1129

E.4.1 CONNECTED TO TRADITIONAL Q -LEARNING

1130

1131

In traditional Q-learning for an MDP, we should minimize the Bellman loss function which iterates over all the states in \mathcal{S} as

1132

1133

$$L = \left\| Q_t(\mathbf{s}, \mathbf{a}) - \sum_{j \in |\mathcal{S}|} P_{s,j}(\mathbf{a}) \left(R(\mathbf{s}, \mathbf{a}) + \gamma \max_b Q_t(j, \mathbf{b}) \right) \right\|^2.$$

1134

1135

1136

1137

1138

1139

1140

1141

1142

1143

1144

1145

1146

1147

1148

1149

1150

1151

1152

1153

1154

1155

1156

1157

1158

1159

1160

1161

1162

1163

1164

1165

1166

1167

1168

1169

1170

1171

1172

1173

1174

1175

1176

1177

1178

1179

1180

1181

1182

1183

1184

1185

1186

1187

Table 4: Symbol definitions in time complexity analysis.

Symbol	Definition
K	History length
N	Dimensional number of the compressed historical trajectory
$ \mathcal{S} $	State number
n_{epoch}	Epoch number in training
d_s	Dimensional number of the state
w	Number of convolution steps
C_{net}	The time complexity of neural networks in No. Aug
$C_{net}^{(A)}$	The time complexity of neural networks in HA3C
C_{sam}	The time complexity from the state number in No. Aug
$C_{sam}^{(A)}$	The time complexity from the state number in HA3C
C_{total}	The total time complexity of No. Aug
$C_{total}^{(A)}$	The total time complexity of HA3C

In this case, from the perspective of PAC, we get a $|\mathcal{S}|$ -based sample complexity as shown in Theorem 2 of Even-Dar & Mansour (2003). The Bellman loss function for DRL is

$$L = \left\| Q_t(\mathbf{s}, \pi_\theta(\mathbf{s})) - \sum_{j \in |\mathcal{S}|} P_{\mathbf{s}, j}(\pi_\theta(\mathbf{s})) \left(R(\mathbf{s}, \pi_\theta(\mathbf{s})) + \gamma \max_\theta Q_t(j, \pi_\theta(j)) \right) \right\|^2.$$

This loss function should be minimized by training the networks to approximate the causal relationships in MDPs, i.e., training the policy network to generate the optimal action as $a^* = \pi_\theta(\mathbf{s})$ and predicting the future state in representation learning. Existing sample efficiency analysis is based on the Bellman loss of the traditional RL approach and thus **do not** consider the sample efficiency of training neural networks in the above causal inference. Our historical augmentation improves sample efficiency for DRL by making the causal inference easier, which is beyond traditional sample efficiency analysis for RL.

Our Bellman loss function is

$$L = \left\| Q_t(\mathbf{z}^{s_k,:}, \pi_\Theta(\mathbf{z}^{s_k,:})) - \sum_{j \in |\mathcal{S}|} P_{\mathbf{s}_k, :, j_k, :}(\pi_\Theta(\mathbf{z}^{s_k,:})) \left(R(\mathbf{s}_k, \pi_\Theta(\mathbf{z}^{s_k,:})) + \gamma \max_\Theta Q_t(j_k, \pi_\Theta(\mathbf{z}^{s_k,:})) \right) \right\|^2.$$

Based on the fact that historical information can simplify the causal relationships in MDPs, our historical augmentation can make policy network π_Θ easier to generate a^* than π_θ and the future state easier to be predicted by representation learning. In this way, sample efficiency can be improved. The detailed analysis is shown in Motivation and the following subsection.

E.4.2 TIME COMPLEXITY ANALYSIS

Based on the above analysis, we perform the time complexity analysis on our HA3C and No. Aug.. First, we list the symbol definitions in Table 4.

Now, we compare the total time complexities of HA3C and No. Aug.. As we can see, C_{total} is based on C_{net} , C_{sam} , and n_{epoch} as

$$C_{total} = C_{net} \times C_{sam} \times n_{epoch}.$$

We also have

$$C_{total}^{(A)} = C_{net}^{(A)} \times C_{sam}^{(A)} \times n_{epoch}.$$

The time complexity of our CNN in our representation is $O(d_s^2 w K N)$, thus

$$C_{net}^{(A)} = C_{net} + O(d_s^2 w K N).$$

When the causal relationships in an MDP cannot be learned by No. Aug., but can be learned by HA3C, we get $C_{sam} = O(|\mathcal{S}|)$ and $C_{sam}^{(A)} = O(1)$.

1188 For example, when training a neural network to predict the next item of each item in a M -order
 1189 Fibonacci sequence as $l(0) = 1, l(1) = 1, l(2) = 2, l(3) = 3, l(4) = 5, \dots$, without considering
 1190 historical information, this neural network may perform brute-force approximation on every item
 1191 in this sequence. In this case, the time complexity from the item number is $O(M)$. However, with
 1192 historical information, only a few consecutive items are needed for the neural network to learn the
 1193 simple linear causal relationship in the Fibonacci sequence, i.e., $l(i+1) = l(i) + l(i-1)$. In this
 1194 case, the time complexity from the item number is $O(1)$.

1195 Therefore, when the time complexity of No Aug. is

$$1198 \quad C_{total} = C_{net} \times |S| \times n_{epoch}.$$

1202 The best time complexity of HA3C is

$$1205 \quad C_{total-best}^{(A)} = (C_{net} + O(d_s^2 w K N)) \times n_{epoch}.$$

1209 E.4.3 ANALYZING SAMPLE EFFICIENCY IN EXPLORATION AND EXPLOITATION

1211 In this subsection, we illustrate the benefit of sample efficiency from history augmentation based on
 1212 two facts:

- 1214 1) Historical augmentation can improve exploration in DRL. The policy can generate different actions
 for different transition trajectories that end with the same state;
- 1216 2) Historical augmentation can also improve exploitation in DRL. History augmentation may simplify
 the causal relationships between the state and the explored high-reward action, thus the policy network
 can effectively learn and then regenerate this action.

1218 The detailed analysis of these two facts is as follows. In the previous DRL methods for MDPs, when
 1219 the policy μ and $s_t = s$ are fixed, we can get only one action by

$$1223 \quad \mathbf{a}_t = \mu(s_t), \quad \mu \in S_1 D.$$

1226 However, based on our history-based policy

$$1229 \quad \mathbf{a}_t = \mu(s_{k,t}), \quad \mu \in S_k D|_{k \geq 2}.$$

1233 \mathbf{a}_t can be changed by the change of the $s_{k-1,t-1}$. We define the set of possible actions from policy
 1234 $\mu \in S_k D$ at state s as A_μ^s and the set of possible k -order trajectories end with state s as S_k^s . As we
 1235 can see, $|A_\mu^s| \leq |S_k^s|$.

1236 Fig. 11 is the causal diagram of regenerating a high-reward action with or without historical aug-
 1237 mentation. For a policy network $\mu_\theta \in S_1 D$ and $\mathbf{a} = \mu_\theta(s)$, we may get $\mathbf{a}^* = \mathbf{a} + \epsilon$ with
 1238 $R(s, \mathbf{a}^*) > R(s, \mathbf{a})$. However, it may be hard to regenerate \mathbf{a}^* by the policy network $\mu_\theta(s)$ because
 1239 the noise ϵ is independent of parameter θ . Fortunately, the causal relationship between $s_{k,t}|_{k \geq 2}$
 1240 and \mathbf{a}^* may be simpler than the causal relationship between s_t and \mathbf{a}^* (See the example in Ap-
 1241 pendix C). In this case, we can effectively learn the policy $\mu_\theta \in S_k D$ to regenerate the \mathbf{a}^* at state s
 by $\mathbf{a}^* = \mu_\theta(s_{k,t})$ (See the example in Fig. 5).

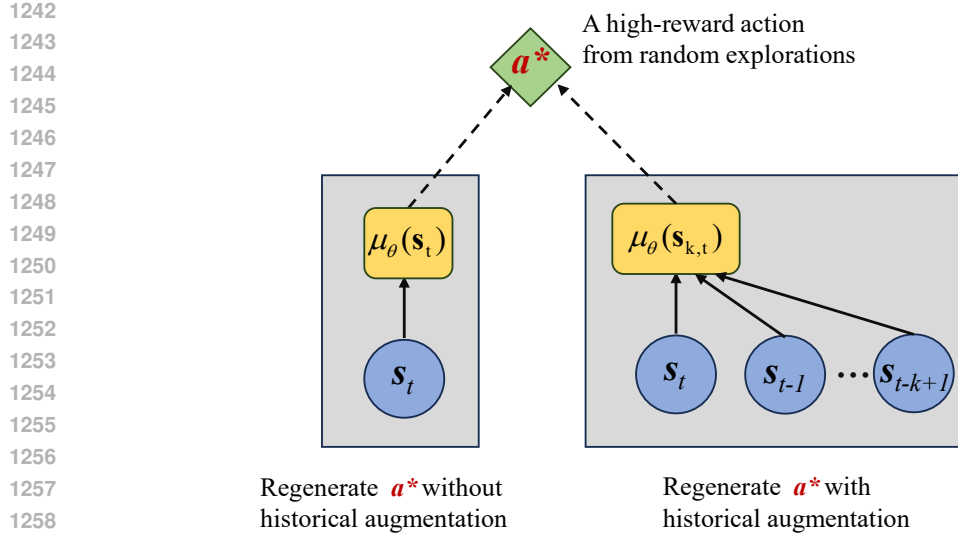


Figure 11: The causal diagram of regenerating a high-reward action with or without historical augmentation. The dashed lines indicate the information needed in the optimization.

F HA3C ALGORITHM

Algorithm 1 Online HA3C

```

1267 Initialize the hyper-parameters and networks
1268 Initialize replay buffer  $\mathcal{B}$ 
1269 for  $episode = 0$  to  $episode_{max}$  do
1270     Collect  $k$ -order transitions by  $\mu_\theta$  and store them in LAP buffer  $\mathcal{B}$ 
1271     if Checkpoint condition then
1272         if  $\mu_\theta$  outperforms  $\mu_{\theta^c}$  then
1273             Update checkpoint networks  $\mu_{\theta^c} \leftarrow \mu_\theta$  and  $f_{\sigma^c} \leftarrow f_\sigma$ 
1274         end if
1275     end if
1276     Sample  $k$ -order transitions from LAP buffer  $\mathcal{B}$ 
1277     Train the encoder  $f_\sigma$  and  $g_\sigma$  by equation 1
1278     Train  $\hat{Q}_{\phi_1}$  and  $\hat{Q}_{\phi_2}$  by equation 3
1279     Train  $\pi_\theta$  by equation 4
1280     if Target update frequency steps have passed then
1281         Update target networks by equation 5
1282     end if
1283 end for

```

G EXPERIMENTAL SETTING

1287 All experiments are run on a single Nvidia 3090 GPU and AMD 5900X CPU. We use the following
1288 software versions:
1289 • Python 3.9.12
1290 • Pytorch 2.0.0 (Paszke et al., 2019)
1291 • CUDA 12.2
1292 • Gymnasium 0.29.1 (Brockman et al., 2016)
1293 • MuJoCo 3.2.3 (Todorov et al., 2012)

1294 The environments in our experiment are shown in Fig. 12 and detailed as follows:
1295 1) Walker2d aims to walk in the forward direction as fast as possible.
1296 2) HalfCheetah aims to run forward as fast as possible.

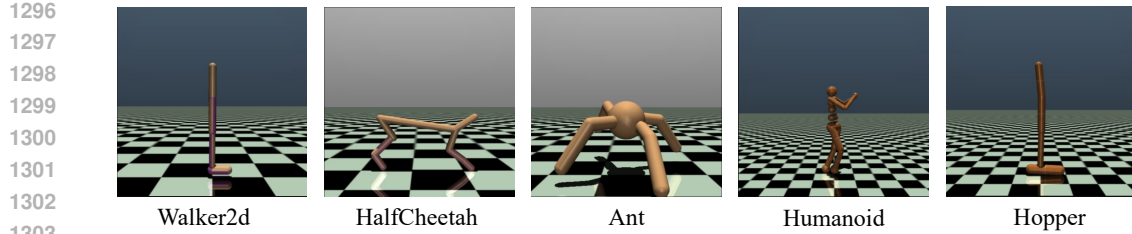


Figure 12: The environments in our experiments.

Table 5: Hyper-parameters.

Parameter	Value	Brief explanation
Start-timesteps	25000	Time steps of the initial random policy is used
Batch-size	512	Batch size for both actor and critic
t_{pol}	3	Policy update frequency
t_{tar}	250	Target update rate
t_{ear}	1	Early assessment episodes for checkpoint operation
t_{lat}	10	Late assessment episodes for checkpoint operation
T_{ear}	750K	Early time steps for checkpoint operation
σ_e	0.1	Std of exploration noise
σ_T	0.05	Std of target policy noise
c	(-0.11,0.11)	Target policy noise clipping
k	6	The length of the considering state sequences
γ	0.99	Discount factor
l_e	0.0006	The learning rate of the encoder network
l_p	0.0003	The learning rate of the actor-network
l_Q	0.0003	The learning rate of the network of the Q -functions
α	0.25	Controlling the amount of prioritization in LAP
P_m	1.1	Minimum priority in LAP

3) Ant aims to coordinate the four legs to move in the forward direction as fast as possible.
 4) Humanoid aims to walk forward as fast as possible without falling over.
 5) Hopper aims to make hops that move in the forward direction as fast as possible.

The compared RL algorithms in our experiment are detailed as follows.

- Online:

- 1) TD3 takes the minimum value between a pair of critic networks to address the overestimation of Q -value and reduces per-update error by delaying policy updates (Fujimoto et al., 2018).
- 2) SAC is an actor-critic algorithm based on the maximum entropy approach. The objective encourages policy stochasticity by augmenting the reward with the entropy at each step (Haarnoja et al., 2018).
- 3) OFE-TD3 increases the input dimensionality of the networks by representation learning to improve the sample efficiency of TD3 (Ota et al., 2020).
- 4) TQC addresses the overestimation of Q -value by the combination of the distributional representation of a critic, truncation of critic prediction, and ensembling of multiple critics (Kuznetsov et al., 2020).
- 5) TD7 is an effective DRL algorithm which combines TD3, state representation learning, checkpoints, prioritized experience replay, and a behaviour cloning term (only used for offline RL) (Fujimoto et al., 2023).

The hyper-parameters of HA3C are shown in Table 5. For Hopper, γ is set as 0.992. Network architecture details are described in Pseudocode 1-3. The optimizer of our networks is Adam Kingma (2015).

```

1350
1351
1352 Critic network:
1353 L1 = Linear(state-dim + action-dim, 256)
1354 L2 = Linear( $z^s$ -dim * 2 + 256, 256)
1355 L3 = Linear(256, 256)
1356 L4 = Linear(256, 1)
1357 Critic forward pass:
1358  $x = \text{Concatenate}([s_t, a_t])$ 
1359  $x = \text{AvgL1Norm}(\text{L1}(x))$ 
1360  $x = \text{Concatenate}([z^{s_{k,t}, a_t}, z^{s_{k,t}}, x])$ 
1361  $x = \text{Elu}(\text{L2}(x))$ 
1362  $x = \text{Elu}(\text{L3}(x))$ 
1363  $\tau(s_{k,t}, a_t) = \text{L4}(x)$ 

```

1364
1365
1366
1367
1368
1369
1370
1371
1372
1373
1374
1375
1376

Pseudocode 3: Encoder Details

1378 **State Encoder f Network:**
1379 Conv = Conv2d(kernel-num=64, kernel-size=(3, state-dim), stride=1)
1380 Pool = MaxPool2d((1, 1))
1381 L1 = Linear(128, 8)
1382 L2 = Linear(state-dim, 256)
1383 L3 = Linear(256+8, 256)
1384 L4 = Linear(256, zs-dim)

1386 **State Encoder f Forward Pass:**
 1387 $x = \text{Conv}(s_{k-1, t-1})$
 1388 $x = \text{Pool}(x)$
 1389 $x = \text{Elu}(\text{L1}(x))$
 1390 $x = \text{AvgL1Norm}(x)$
 1391 $y = \text{Elu}(\text{L2}(s_t))$
 1392 $x = \text{Concatenate}([x, y])$
 1393 $x = \text{Elu}(\text{L3}(x))$
 1394 $z^{s_{k, t}} = \text{AvgL1Norm}(\text{L4}(x))$

State-Action Encoder g Network:
 L1 = Linear(action-dim + z^s -dim, 256)
 L2 = Linear(256, 256)
 L3 = Linear(256, z^s -dim)

1398 L3 = Linear(256, $z^{\text{v}}\text{-dim}$)
 1399 **State-Action Encoder g Forward Pass:**
 1400 $x = \text{Concatenate}([\mathbf{a}_t, \mathbf{z}^{s_{k,t}}])$
 1401 $x = \text{Elu}(\text{L1}(x))$
 1402 $x = \text{Elu}(\text{L2}(x))$
 1403 $\mathbf{z}^{s_{k,t}, a_t} = \text{L3}(x)$

```

1404
1405 Pseudocode 2: Actor network Details
1406
1407 Actor network:
1408  $L1 = \text{Linear}(\text{state-dim}, 256)$ 
1409  $L2 = \text{Linear}(z^s\text{-dim} + 256, 256)$ 
1410  $L3 = \text{Linear}(256, 256)$ 
1411  $L4 = \text{Linear}(256, \text{action-dim})$ 
1412 Actor forward pass:
1413  $x = \text{AvgL1Norm}(L1(s_t))$ 
1414  $x = \text{Concatenate}([z^{s_{k,t}}, x])$ 
1415  $x = \text{ReLU}(l1(x))$ 
1416  $x = \text{ReLU}(l2(x))$ 
1417  $a_t = \text{Tanh}(l3(x))$ 
1418
1419
1420
1421
1422
1423
1424
1425
1426
1427
1428
1429
1430
1431
1432
1433
1434
1435
1436
1437
1438
1439
1440
1441
1442
1443
1444
1445
1446
1447
1448
1449
1450
1451
1452
1453
1454
1455
1456
1457

```

H SUPPLEMENTARY EXPERIMENT

H.1 BIPEDAWALKER EXPERIMENT

To illustrate the benefit of history augmentation for complex MDP tasks, we test HA3C and No Aug. (HA3C without historical augmentation) on BipedalWalker and BipedalWalker-hardcore tasks. In BipedalWalker a robot is trained to move forward with slightly uneven terrain. Compared with BipedalWalker, BipedalWalker-hardcore is a more complex task, where the above robot is trained to move forward with ladders, stumps, and pitfalls. Therefore, the causal relationships in the transitions of BipedalWalker-hardcore are more complex than those in the transitions of BipedalWalker. The environments and learning curves are shown in Fig. 13 and the numerical results are shown in Table 6.

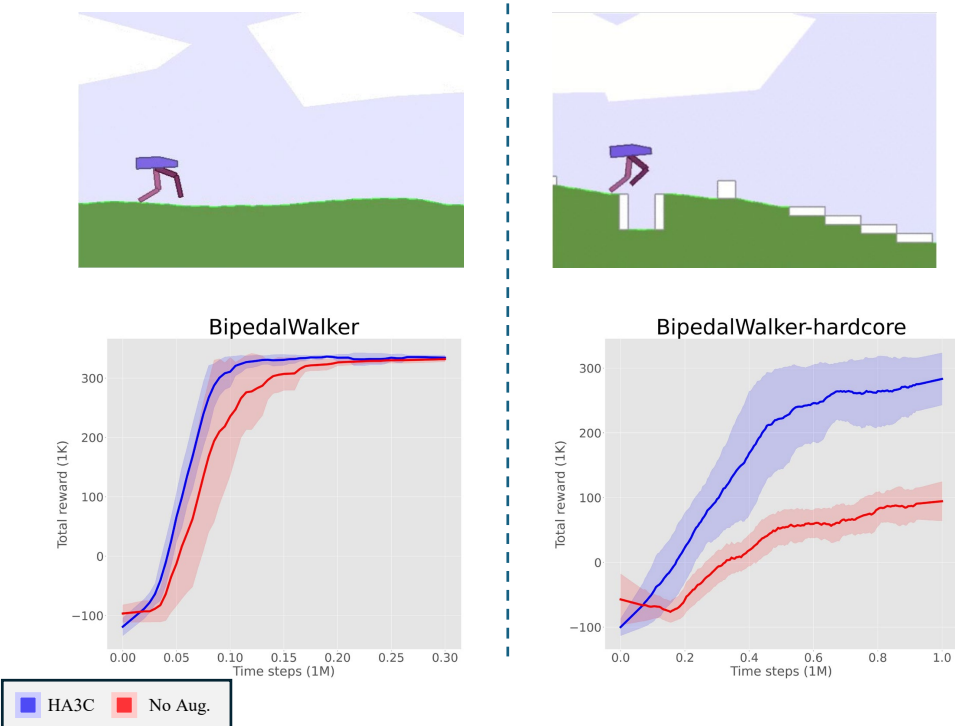


Figure 13: The environments and learning curves on BipedalWalker and BipedalWalker-hardcore tasks.

1458
1459
1460

Table 6: The average highest returns of HA3C and No Aug. on BipedalWalker and BipedalWalker-hardcore tasks.

1461
1462
1463
1464
1465
1466
1467
1468
1469
1470

Algorithm	BipedalWalker	BipedalWalker-hardcore
HA3C	332 ± 27	316 ± 19
No Aug.	325 ± 31	171 ± 21

As we can see, although, both HA3C and No Aug. can get the high cumulative rewards in BipedalWalker, only HA3C can get the high cumulative rewards in BipedalWalker-hardcore. This is because by historical augmentation our HA3C can simplify the causal relationships in the transitions of BipedalWalker-hardcore.

1471
1472
1473
1474
1475
1476
1477
1478
1479
1480

H.2 DEEP MIND CONTROL SUITE EXPERIMENT

In this subsection, we evaluate our HA3C on five DMC tasks including ball_in_cup-catch, walker-run, quadruped-run, cheetah-run, and reacher-hard (Tassa et al., 2018). The compared algorithms are TD3 (Fujimoto et al., 2018) and TD7 (Fujimoto et al., 2023). For all algorithms, each task runs 10 instances with 10^6 time steps with different random seeds. In each instance, the evaluation is performed every 5000 time steps. Some parameters are changed as follows. For quadruped-run, l_e is set as 0.0006, σ_T is set as 0.06, and c is set as $(-0.12, 0.12)$. For other tasks, l_e is set as 0.0005 and c is set as $(-0.1, 0.1)$. The learning curves are shown in Fig. 14 and the numerical results at 300K time step and 1M time step are shown in Table 7.

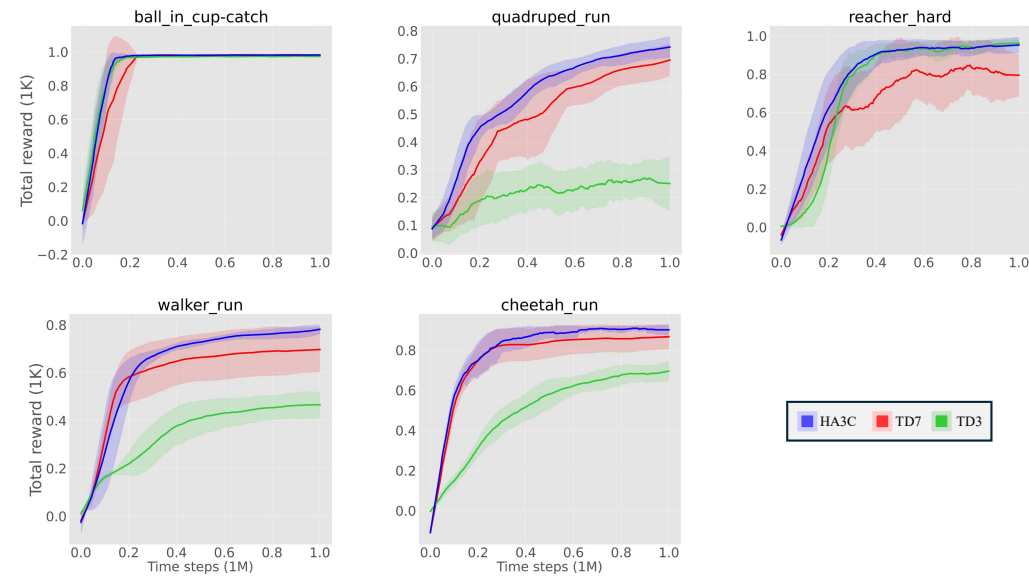
1500
1501

Figure 14: Learning curves of different RL algorithms on the deep mind control suite tasks.

1502
1503
1504
1505
1506
1507

As we can see, in most cases, HA3C has higher cumulative rewards than the compared algorithms. For walker-run, quadruped-run, and reacher-hard, HA3C outperforms the compared algorithms in terms of both the early performance and the final performance. For ball_in_cup-catch and cheetah-run, HA3C outperforms all of the compared algorithms in the final performance but the average return of HA3C is lower than the average return of TD7 in the early performance.

1508
1509

H.3 COMBINING HISTORICAL REPRESENTATION LEARNING WITH SAC

1510
1511

In this subsection, we combine our historical representation learning with SAC to construct HA3C-SAC method (Haarnoja et al., 2018). Then we evaluate HA3C-SAC on three MuJoCo control tasks including Walker2d, Humanoid, and Hopper. The compared methods includes the original

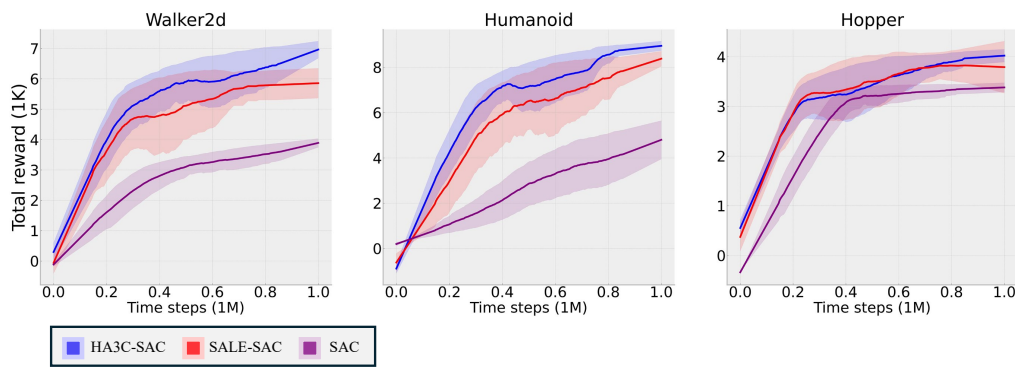
1512

1513 Table 7: The average highest returns over 10 instances on the deep mind control suite tasks at 400K
1514 and 1M time steps.

Algorithm	Time step	ball_in_cup-catch	walker-run	quadruped-run	cheetah-run	reacher-hard
TD3	400K	981 \pm 2	387 \pm 71	331 \pm 65	550 \pm 76	971 \pm 3
	1M	985 \pm 1	481 \pm 54	444 \pm 22	729 \pm 39	979 \pm 1
TD7	400K	990 \pm 2	654 \pm 96	531 \pm 69	836 \pm 75	879 \pm 91
	1M	991 \pm 1	706 \pm 95	703 \pm 54	868 \pm 56	979 \pm 5
HA3C	400K	989 \pm 2	713 \pm 41	598 \pm 36	834 \pm 108	976 \pm 5
	1M	992 \pm 1	789 \pm 19	758 \pm 24	916 \pm 5	985 \pm 5

1524

1525

1526 SAC and SALE-SAC, which combines the representation learning with SAC without historical
1527 augmentation (Fujimoto et al., 2023). The learning curves are shown in Fig. 15 and the numerical
1528 results are shown in Table 8.

1529

1530

1531 Figure 15: Learning curves of different RL algorithms on SAC, SALE-SAC, and HA3C-SAC on
1532 Mujoco tasks.

1533

1534

1535

1536

1537

1538

1539

1540

1541

1542

1543

1544

1545

1546

1547

Table 8: The average highest returns on Mujoco control tasks at 400K and 1M time steps.

Algorithm	Time step	Walker2d	Humanoid	Hopper
SAC	400K	2843 \pm 148	2268 \pm 905	3195 \pm 33
	1M	3921 \pm 163	5498 \pm 131	3422 \pm 86
SALE-SAC	400K	5414 \pm 377	6430 \pm 191	3515 \pm 125
	1M	6021 \pm 492	8368 \pm 330	4038 \pm 126
HA3C-SAC	400K	5796 \pm 395	7112 \pm 339	3566 \pm 39
	1M	6950 \pm 623	9047 \pm 238	4131 \pm 48

1556

1557

1558

1559

As we can see, HA3C-SAC outperforms SAC and SALE-SAC on the three Mujoco control tasks.
The above results and the results Section 5.1 illustrate that our historical representation learning is
robust to different algorithms and tasks.

1560

1561

H.4 THE COMPARISON BETWEEN CNN AND LSTM ON HA3C

1562

1563

1564

1565

In this subsection, a new algorithm, HA3C-LSTM, is constructed to learn the historical representation
by the LSTM architecture (Hochreiter & Schmidhuber, 1997). Like HA3C, HA3C-LSTM compresses
historical trajectories into an 8-dimensional space in the representation learning. The learning curves
are shown in Fig. 16 and the numerical results are shown in Table 9.

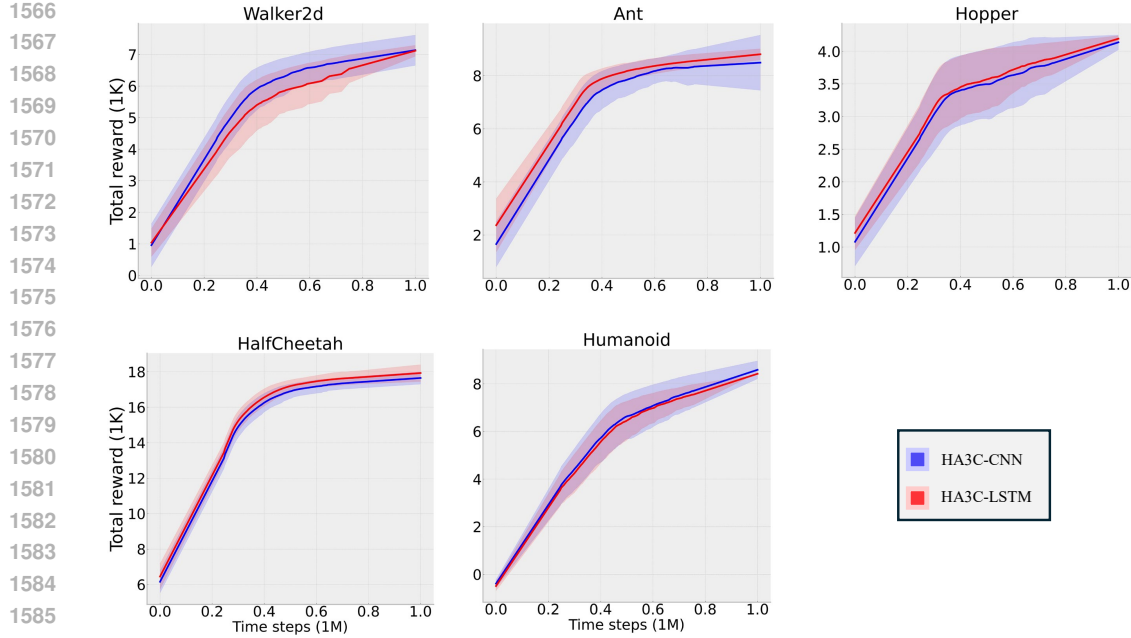


Figure 16: Learning curves of HA3C-CNN and HA3C-LSTM on Mujoco tasks.

Table 9: The average highest returns on Mujoco control tasks at 300K and 1M time steps.

Algorithm	Time step	Walker2d	HalfCheetah	Ant	Humanoid	Hopper
HA3C-CNN	300K	6036 \pm 429	16415 \pm 437	7488 \pm 389	6248 \pm 188	3594 \pm 106
	1M	7324 \pm 433	17863 \pm 515	8771 \pm 362	8572 \pm 446	4110 \pm 105
HA3C-LSTM	300K	5809 \pm 394	16637 \pm 334	7514 \pm 442	6185 \pm 273	3734 \pm 178
	1M	7242 \pm 409	18160 \pm 413	8784 \pm 552	8259 \pm 279	4212 \pm 64

Overall, the performances of HA3C and HA3C-LSTM are competitive (similar). HA3C slightly outperforms HA3C-LSTM on Walker2d and Humanoid. HA3C-LSTM slightly outperforms HA3C on HalfCheetah, Hopper, and Ant. However, as we can see from Fig. 18, HA3C-CNN runs faster than HA3C-LSTM. Therefore, we choose CNN architecture in our historical representation learning.

H.5 THE COMPARISON BETWEEN HA3C AND CROSSQ

In this subsection, we compare HA3C with CrossQ on Mujoco benchmark with 3M time steps in the following. The learning curves are shown in Fig. 17 and the numerical results are shown in Table 10.

Table 10: The average highest returns on Mujoco control tasks at 300K and 3M time steps.

Algorithm	Time step	Walker2d	HalfCheetah	Ant	Humanoid	Hopper
CrossQ	300K	6036 \pm 429	10192 \pm 1958	5712 \pm 684	9261 \pm 473	3551 \pm 62
	3M	7324 \pm 433	14251 \pm 2020	7913 \pm 459	11978 \pm 510	3780 \pm 200
HA3C	300K	6036 \pm 429	16415 \pm 437	7488 \pm 389	6248 \pm 188	3594 \pm 106
	3M	8563 \pm 829	18687 \pm 683	9794 \pm 891	11521 \pm 412	4413 \pm 59

We can see that 1) with the help of our historical representation learning, HA3C significantly outperforms CrossQ on Walker2d, HalfCheetah, Ant and Hopper at 300K and 3M time steps; 2) CrossQ significantly outperforms HA3C on Humanoid at 300K timesteps and slightly outperforms HA3C at 3M timesteps.

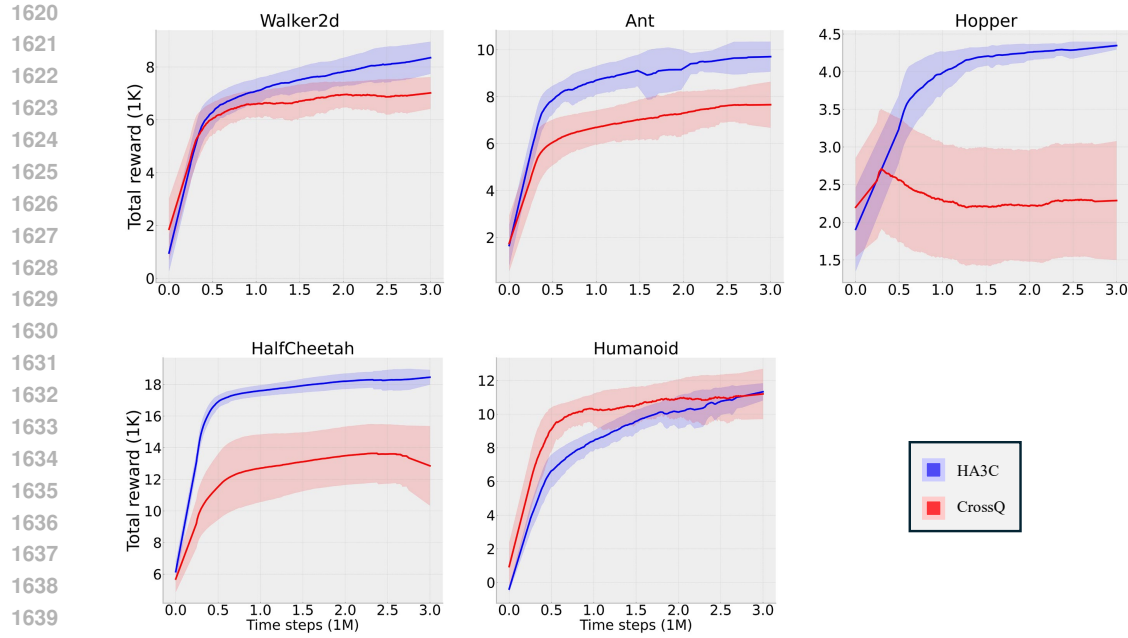


Figure 17: Learning curves of HA3C and CrossQ on Mujoco tasks.

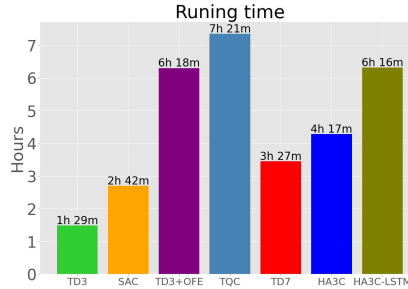


Figure 18: Running times of different algorithms for 1M time steps.

H.6 RUNNING TIME

To understand the computational cost of HA3C, we compare the running times of different algorithms with identical computational resources in HalfCheetah control task. The result is shown in Fig. 18. As we can see, the computational cost of HA3C is less than the computational costs of TD3+OFE and TQC but is more than the computational costs of TD3, SAC, and TD7.

The computational cost of HA3C-LSTM is more than that of HA3C. From Section H.4, we can see that the performances of HA3C and HA3C-LSTM are similar. Therefore, we choose CNN architecture in our historical representation learning.

Fig. 19 presents the visual results and the histogram of the transitions in HA3C and No Aug. The collected states of each control task are mapped together by UMAP. The max learning step is 4×10^5 and each state is coloured by the reward of reaching it.

As we can see, in Walker2d, Ant, and Humanoid, the high-reward states from HA3C are more than those from No Aug. This result illustrates that the sample efficiency of DRL can be effectively improved by learning the state representations with historical augmentation.

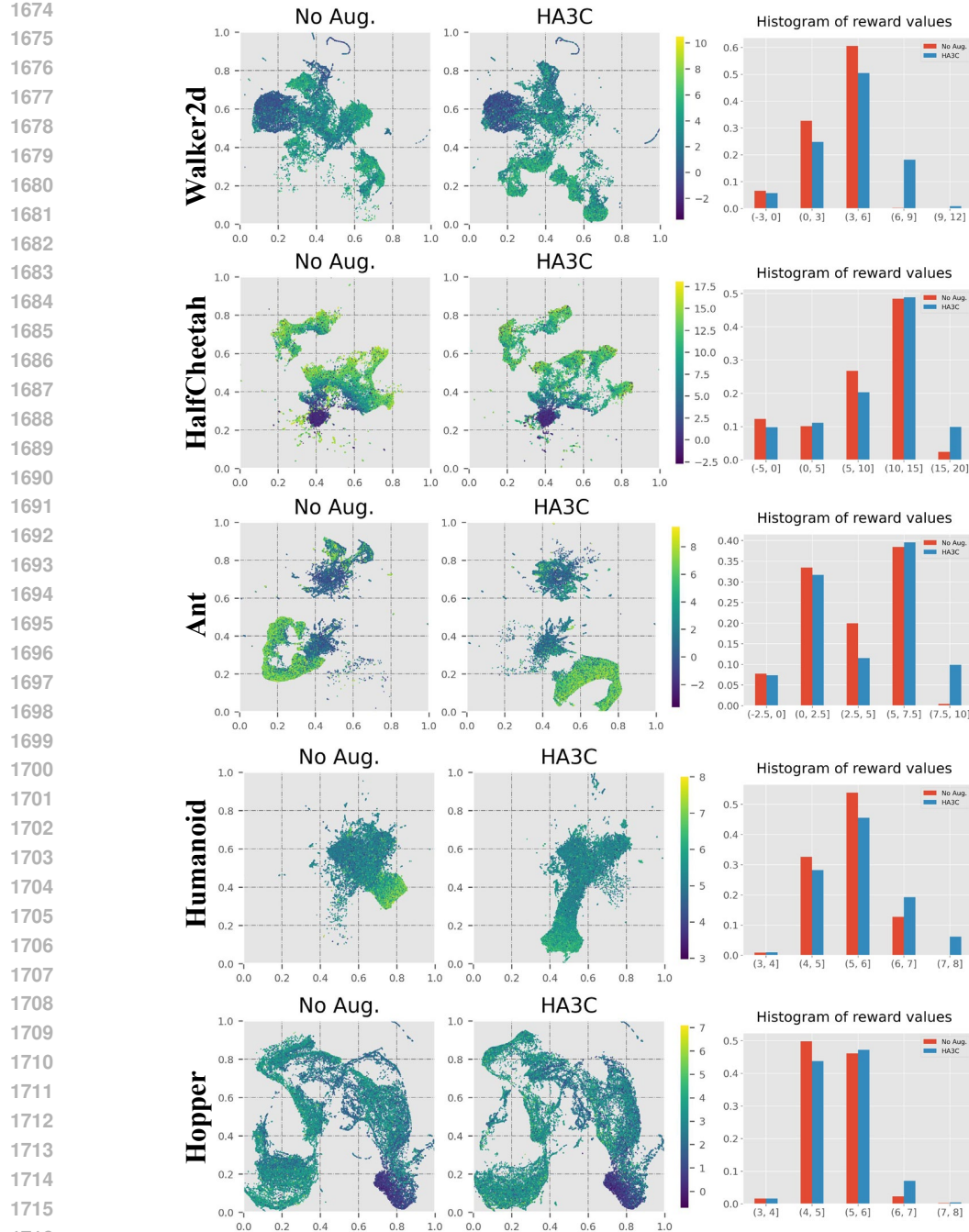


Figure 19: Visualized results of the explored states in No Aug. and HA3C.

I THE USAGE OF LARGE LANGUAGE MODELS

In this paper, large language models are used for grammar checking and polishing.